HHS Public Access

Author manuscript

*Sci Immunol*. Author manuscript; available in PMC 2023 March 30.

Published in final edited form as:

*Sci Immunol*. 2022 September 30; 7(75): eabq7432. doi:10.1126/sciimmunol.abq7432.

# cDC1 coordinate innate and adaptive responses in the omentum required for T cell priming and memory

**David A. Christian**[1], **Thomas A. Adams II**[2], **Lindsey A. Shallberg**[1], **Anthony T. Phan**[1], **Tony E. Smith**[3], **Mosana Abraha**[2], **Joseph Perry**[1], **Gordon Ruthel**[1], **Joseph T. Clark**[1], **Gretchen Harms Pritchard**[1], **Lillian R. Aronson**[1,4], **Selamawit Gossa**[5], **Dorian B. McGavern**[5], **Ross M. Kedl**[6], **Christopher A. Hunter**[1,#]

[1]Department of Pathobiology, University of Pennsylvania, Philadelphia, PA 19104

[2]Department of Chemical Engineering, McMaster University, Hamilton, Ontario

[3]Department of Electrical and Systems Engineering, University of Pennsylvania, Philadelphia, PA 19104

[4]Section of Surgery, Department of Clinical Studies, University of Pennsylvania, Philadelphia, PA 19104

[5]Viral Immunology and Intravital Imaging Section, National Institute of Neurological Disorders and Stroke, National Institutes of Health, Bethesda, Maryland 20814

[6]Department of Immunology & Microbiology, University of Colorado Anschutz Medical Campus, Aurora, CO 80045

## Abstract

In the peritoneal cavity the omentum contains fat associated lymphoid clusters (FALCs) whose role in response to infection is poorly understood. After intraperitoneal immunization with *Toxoplasma gondii*, conventional type 1 dendritic cells (cDC1) were critical to induce innate sources of IFN-γ and cellular changes in the FALCs. Unexpectedly, infected peritoneal macrophages that migrated into the FALCs primed $CD8^+$ T cells. While T cell priming was cDC1-independent, these DC were required for maximal $CD8^+$ T cell expansion. An agent-based computational model and experimental data highlighted that cDC1 impacted the magnitude of the proliferative burst and promoted $CD8^+$ T cell expression of nutrient uptake receptors and cell survival. Thus, although FALCs lack the organization of secondary lymphoid organs, cDC1 resident in this tissue coordinate innate responses to microbial challenge and provide secondary signals required for T cell expansion and memory formation.

[#]Correspondence: Christopher A. Hunter. Department of Pathobiology, University of Pennsylvania, 380 South University Ave, Rm 313 Hill Pavilion, Philadelphia, PA 19104. Telephone: (215) 573-7772, Fax: (215) 746-2295 chunter@vet.upenn.edu.

AUTHOR CONTRIBUTIONS

Conceptualization, D.A.C., T.A.A., A.T.P., and C.A.H.; Methodology, D.A.C., T.E.S., and T.A.A.; Software, T.A.A., T.E.S., and M.A.; Formal Analysis, D.A.C., T.A.A. and T.E.S.; Investigation, D.A.C., T.A.A., L.A.S., M.A., J.P., J.T.C, G.H.P, and L.R.A.,; Resources, S.G. and D.B.M.; Writing – Original Draft, D.A.C. and C.A.H.; Writing – Review & Editing, D.A.C., A.T.P., and C.A.H.; Visualization, D.A.C. and G.R.; Supervision, D.A.C. and C.A.H.; Project Administration, D.A.C. and C.A.H.; Funding Acquisition, D.A.C., R.M.K, and C.A.H.

COMPETING INTERESTS

D.A.C. and T.A.A. have filed a patent on the STORE model. The other authors declare that they have no competing interests.

## ONE-SENTENCE SUMMARY:

cDC1 are not required for T cell priming but coordinate immune responses in the omentum to generate protective T cell responses.

## INTRODUCTION

Clusters of immune cells in white adipose tissue (WAT) form fat-associated lymphoid clusters (FALCs) (1, 2) that provide protective immunity following a breach in local lymphatics or mucosal barrier sites (3–6). In response to inflammation within serous cavities, FALCs increase in size as leukocytes from the blood or cells from the cavities access these structures (1, 5, 7). In the peritoneum, the omentum is composed of mesothelial sheets that enclose adipose tissue densely populated with FALCs (termed milky spots, MS) that are enriched for B cells but also other immune cells (8). These vascularized MS associate with stomata in the mesothelial layer of the omentum and allow entry of inflammatory cells into the peritoneum (5, 6, 9, 10), but are also a site of cellular egress and antigen drainage from the peritoneum (6, 7, 9–11). While soluble antigen from the peritoneum can drain to the mediastinal and parathymic lymph nodes (LNs) (12), cells and particulates drain almost entirely to the omentum (9, 11). In higher vertebrates, the MS in the omentum contribute to humoral responses (7), but are less organized compared to conventional secondary lymphoid organs (SLOs) (8). The reduced complexity of FALCs and differences in the stromal cell network have contributed to the idea that these sites have a secondary role in the induction of immune responses.

Within LNs the positioning of cDC is critical for the efficient capture and presentation of antigen to generate T cell responses (13–15). This localization is of particular relevance to cDC1 that cross-present exogenous antigen to $CD8^+$ T cells (16, 17). However, studies with vaccinia virus (VV) concluded that in LN cDC1 were not required for priming, but rather that uninfected cDC1 allow communication between $CD4^+$ and $CD8^+$ T cells that shape $CD8^+$ T cell differentiation (13). This role for cDC1 as a platform to help $CD8^+$ T cell responses is apparent in other systems (15, 17), but less is known about the localization and function of cDC in the FALCs. Intraperitoneal (i.p.) infection with a live, replication-deficient strain of *T. gondii* results in DC-dependent parasite-specific $CD8^+$ and $CD4^+$ T cell responses (18, 19). In the present study, a replication-deficient strain of *T. gondii* that expresses ovalbumin (OVA) and Cre recombinase was combined with a Cre-sensitive reporter mouse to define the events involved in $CD8^+$ T cell priming in the omentum. These data sets formed the basis for an agent-based model to predict how perturbations in priming would impact $CD8^+$ T cell responses. Together, these studies demonstrate that cDC1 mediate inflammatory changes in the FALCs, and – although infected macrophages prime $CD8^+$ T cells – cDC1 in the FALCs provide secondary signals required for T cell expansion and memory formation.

# RESULTS

## Immunization alters organization of the omental MS

Injection of the CPS strain of *T. gondii* i.p. results in rapid infection of the resident cells. To track host-parasite interactions, CPS that express mCherry and inject Cre recombinase into host cells (CPS-Cre-mCherry) were combined with Cre-sensitive Ai6 reporter mice to identify cells that had phagocytosed parasites (Toxo$^{+}$ZsGreen$^{-}$), had been infected (Toxo$^{+}$ZsGreen1$^{+}$), or been injected with Cre (Toxo$^{-}$ZsGreen$^{+}$) (20, 21). In the first 2 days post-immunization (dpi), infected cells had moved from the peritoneum to the omentum but were rare in the draining parathymic and mediastinal lymph nodes (DLN) (Fig. 1A). By 2 dpi in the omentum there was an influx of large peritoneal macrophages (LPM), MHCII$^{+}$ monocytes, and macrophages (Mϕ) (Fig. 1B, C), and CD64$^{+}$ LPM and Mϕ composed the majority of infected or injected cells (Fig. 1D, E). Imaging revealed the MS contained distinct regions enriched for B cells and a central T cell zone (Fig. 1F–G). Reticular cells and reticular fibers formed an extensive network, and infected cells were present in a mantle of CD11b$^{+}$ myeloid cells (Fig. 1H). The use of *Lyz2*-Cre mice interbred with Ai6 reporters (*Lyz2*$^{Ai6}$), indicated that this mantle was largely composed of monocytes (fig. S1A–F). Infected ZsGreen$^{+}$ macrophages were observed in regions enriched with T and B cells (Fig. 1I–J) but not outside the MS (fig. S1G). Thus, after CPS immunization infected macrophages migrate from the peritoneum into the MS accompanied by monocyte recruitment.

## cDC1 coordinate innate changes in the MS

cDC1 are the source of IL-12 that stimulates group 1 ILCs to produce IFN-γ required for resistance to *T. gondii* (22). To determine the impact of cDC1 and IL-12 on the immune response to CPS, *Batf3*$^{-/-}$ mice that lack cDC1 (fig. S2A–B) and *Il12b*$^{-/-}$ mice were compared to WT mice. *Batf3*$^{-/-}$ and *Il12b*$^{-/-}$ mice had a major defect in recruitment of Ly6C$^{HI}$ monocytes into the omentum (Fig. 2A–C, fig. S2C) and peritoneum (fig. S2D–F), and reduced NK and ILC1 production of IFN-γ (Fig. 2D–F, fig. S2G–I). Comparison of immunized Rag2$^{-/-}$ and Rag2$^{-/-}$γc$^{-/-}$ mice (lacking ILCs) revealed that ILCs are required to recruit monocytes to the peritoneum (fig. S2J–K). Moreover, CPS immunization induces a loss of LPM in the peritoneum associated with their migration to the omentum that was dependent on cDC1 and IL-12 (fig. S2L–M). Nevertheless, infected and injected cells accumulated in the MS of Ai6 and Ai6/*Batf3*$^{-/-}$ mice (Fig. 2G–I), indicating that infected LPM migrated into the MS in the absence of cDC1 (Fig. 2J). Thus, cDC1 coordinate the recruitment of monocytes into the omentum and peritoneum and resident macrophages from the peritoneum into the MS, but migration of infected cells into the omentum is cDC1-independent.

## CD8$^{+}$ T cell priming occurs in the omentum

The presence of infected macrophages in an area rich in T cells in the MS suggested that this may be a site of T cell priming. Therefore, CPS parasites that expressed OVA (CPS-OVA) were combined with OT-I T cells that transiently expressed Nur77$^{GFP}$ after TCR engagement (OT-I/Nur77$^{GFP}$). CellTrace Violet (CTV) labeled OT-I/Nur77$^{GFP}$ T cells were transferred intravenously (i.v.) into congenically distinct hosts that were then immunized

with CPS-OVA or heat-killed (HK) CPS-OVA. At 3 dpi, only CPS-OVA induced marked Nur77$^{GFP}$ expression and proliferation in the omentum (Fig. 3A–B) with low levels of OT-I T cell activation observed in the DLN (fig. S3A). Omentectomy at 2 dpi resulted in a 70% decrease in the number of parasite-specific CD8$^{+}$ and CD4$^{+}$ T cells in the peritoneum at 10 dpi (fig. S3B). While this surgical intervention would result in a reduced parasite antigen load, this result is consistent with the omentum as a site of antigen drainage and T cell priming. Furthermore, i.p. transfer of OT-I/Nur77$^{GFP}$ T cells followed by immunization with CPS or CPS-OVA revealed that by 18 hours post-immunization only the CPS-OVA resulted in upregulation of CD69 and Nur77$^{GFP}$ (Fig. 3C–D).

Next, Ai6 mice were immunized with CPS-Cre-OVA-mCherry parasites and 18 hours post-immunization (hpi) CTV-labeled OT-I/Nur77$^{GFP}$ T cells along with CellTrace Yellow-labeled P14 T cells (an internal control specific for the gp33 peptide of LCMV) were transferred i.p. into immunized Ai6 mice. Intravital imaging of the omentum showed that OT-I/Nur77$^{GFP}$ T cells had a significantly slower migration speed and a larger proportion exhibiting an arrested behavior around infected ZsGreen$^{+}$ cells than the P14 T cells (Fig. 3E). Occasional stalling (a hallmark of APC:T cell interactions) of OT-I/Nur77$^{GFP}$ T cells in direct contact with an infected ZsGreen$^{+}$ cell was observed (Fig. 3F). To assess whether LPM could prime CD8$^{+}$ T cells, uninfected (ZsGreen$^{-}$) and infected (ZsGreen$^{+}$) LPM from CPS-Cre-OVA-mCherry immunized Ai6 mice were purified and co-cultured with CTV-labeled OT-I/Nur77$^{GFP}$ T cells. While LPM from naïve controls or uninfected LPM from vaccinated mice did not activate the OT-I/Nur77$^{GFP}$ T cells, infected LPM induced OT-I T cells to express Nur77$^{GFP}$ and undergo division (Fig. 3G–H). Likewise, when mice lacking β2-microglobulin (β2M) in macrophages (*Lyz2*-β2M mice) (fig. S3C) were vaccinated, the fraction of CD69$^{+}$Nur77$^{GFP+}$ OT-I T cells was significantly decreased (Fig. 3I–J).

The ability of activated T cells to cluster around APCs is a hallmark of T cell priming. Imaging of the MS at 18 hpi with CPS-Cre-OVA-mCherry revealed clusters of OT-I T cells in the T cell zone (Fig. 3K) that contained CTV$^{+}$Nur77$^{GFP+}$ OT-I T cells while CTV$^{+}$Nur77$^{GFP-}$ OT-I T cells appeared more dispersed (Fig. 3L). Random permutation tests of clustering were employed using K-function statistics to determine that Nur77$^{GFP+}$ OT-I T cells exhibited significant clustering compared to the total OT-I T cell population at a radius of $k = 4$ μm (Fig. 3M). This analysis also revealed that Nur77$^{GFP+}$ OT-I T cells were dispersed away from ZsGreen$^{+}$ macrophages in Ai6 mice (Fig. 3N, P), and instead clustered around cDC1 (*Snx22*$^{GFP+}$ (23), Fig. 3O) at radii larger than 5 μm (Fig. 3Q, Movie S1). Thus, infected LPM present antigen via MHC Class I to naive CD8$^{+}$ T cells and these activated CD8$^{+}$ T cells then form secondary clusters around cDC1.

## cDC1 are required for CPS-induced T cell responses

To assess the role of cDC1 in the generation of CPS-induced T cell responses, WT and *Batf3*$^{-/-}$ mice were vaccinated and assessed at 8–11 dpi or >30 dpi. At acute time points, *Batf3*$^{-/-}$ mice had a reduced population of parasite-specific CD4$^{+}$ and CD8$^{+}$ T cells in the spleen (Fig. 4A–D). Moreover, the ability of CPS-OVA to expand OT-I T cells was significantly decreased in *Batf3*$^{-/-}$ mice (Fig. 4E). Similar results were observed with *Irf8*

*+32*$^{-/-}$ mice, that lack cDC1 but are *Batf3* sufficient (24) (Fig. 4F). The lack of cDC1 also resulted in a significant decrease in the number (Fig. 4G–H) and altered expression of CXCR3 and KLRG1 by parasite-specific CD8$^{+}$ T cells in the peritoneum (Fig. 4I–J). This phenotypic difference was T cell-extrinsic as it was also observed in OT-I T cells primed in *Batf3*$^{-/-}$ mice (Fig. 4K–L). By 30 dpi the endogenous parasite-specific CD8$^{+}$ T cell population was still reduced in *Batf3*$^{-/-}$ and *Irf8 +32*$^{-/-}$ mice (Fig. 4M–N). When CPS-immunized mice were challenged with the virulent RH strain of *T. gondii*, WT mice were completely protected while immunized *Batf3*$^{-/-}$ mice (Fig. 4O) or *Irf8 +32*$^{-/-}$ mice succumbed to this challenge (fig. S3D).

To compare the fitness of memory CD8$^{+}$ T cells generated in the absence of cDC1, congenically distinct OT-I T cells were transferred into WT and *Batf3*$^{-/-}$ mice that were then immunized with CPS-OVA. At 42 dpi, memory OT-I T cells were isolated from WT and *Batf3*$^{-/-}$ hosts, mixed 1:1, and transferred into WT mice that were then infected with an OVA-expressing avirulent strain of *T. gondii* (Pru-OVA). Prior to transfer the OT-I T cells from *Batf3*$^{-/-}$ hosts had a reduced central memory CD8$^{+}$ T cell population (fig. S3E). Following re-challenge, CD45.1$^{+}$ OT-I T cells from the *Batf3*$^{-/-}$ hosts had a significant defect in expansion compared to CD45.1.2$^{+}$ OT-I T cells from WT mice (Fig. 4P–Q, fig. S3F). Thus, the absence of cDC1 results in a defect in number and phenotype of parasite-specific CD4$^{+}$ and CD8$^{+}$ T cells at acute and memory time points and a defect in resistance to rechallenge.

## Role of IL-12 and cDC1 in CD4$^{+}$ and CD8$^{+}$ T cell expansion

Because cDC1 are an important source of IL-12 that promotes T cell responses during toxoplasmosis (22), experiments were performed to test if treatment of *Batf3*$^{-/-}$ mice with IL-12 would restore the parasite-specific T cell response. In WT mice, treatment with rIL-12 did not affect the AS15:I-A$^{b+}$ CD4$^{+}$ T cell response, but restored the frequency and enhanced numbers of these CD4$^{+}$ T cells in *Batf3*$^{-/-}$ mice (Fig. 5A–C). In contrast, treatment of *Batf3*$^{-/-}$ mice with rIL-12 had a small but insignificant impact on the frequency, number, and differentiation of tgd057:K$^{b+}$ CD8$^{+}$ T cells (Fig. 5D–I). Thus, cDC1 have an IL-12-independent role in the induction of a parasite-specific CD8$^{+}$ T cell response.

To investigate how the absence of cDC1 impacted the T cell response, OT-I/Nur77$^{GFP}$ T cells were transferred into WT and *Batf3*$^{-/-}$ mice that were then immunized with CPS-OVA. At 18 hpi, OT-I/Nur77$^{GFP}$ T cells showed similar levels of activation (CD69$^{+}$Nur77$^{GFP+}$) in the omentum of WT and *Batf3*$^{-/-}$ mice (Fig. 6A–B), but Nur77$^{GFP+}$ OT-I T cells did not cluster in *Batf3*$^{-/-}$ mice (Fig. 6C–D). Next, *Xcr1*-β2M mice that lack β2M on cDC1 (Fig. 6E–F) showed a decreased acute OT-I T cell response after CPS-OVA vaccination (Fig. 6G–H). Analysis of the kinetics of CTV-labelled OT-I T cell response in multiple tissues of WT and *Batf3*$^{-/-}$ mice revealed that OT-I T cells were not detected in large numbers in the DLN or spleen until they had undergone several divisions (fig. S3G). In the omentum at 2 dpi the activation and proliferative response of OT-I T cells in the *Batf3*$^{-/-}$ and WT mice were similar. However, by 3 dpi a significantly smaller fraction of OT-I T cells had divided in the *Batf3*$^{-/-}$ mice (Fig. 6I–J). Thus, in the absence of cDC1 there is no defect in initial

activation of OT-I T cells, but cDC1 are required to present antigen to generate a maximal $CD8^+$ T cell response.

## Agent-based modeling of T cell priming and expansion

To understand how absence of cDC1 affects the $CD8^+$ T cell response, an agent-based stochastic model – the STochastic Omentum REsponse (STORE) model – was developed to identify how perturbations to the system would affect $CD8^+$ T cell responses. The different steps of the T cell response are mostly described by probability distribution functions based on literature values (Fig. 7A, Supplementary Methods). Six model parameters were derived from our experiments: 1) the number of transferred OT-I, 2) the ratio of transferred OT-I to the number of APCs generated by CPS-OVA ($r_{AP}$), the probabilities of 3) an OT-I and APC binding ($p_{AP,bind}$), 4) an APC leaving the system ($p_{BP,leave}$), 5) cells in divisions 3–6 leaving ($p_{EH,leave}$), and 6) cells in divisions 7–8+ leaving ($p_{IJ,leave}$). After CPS-OVA immunization, the use of this model in a dynamic simulation tracked the fate of individual OT-I T cells in the omentum of each mouse for 8 days. The stochasticity and fidelity of the STORE model are illustrated in Fig. 7B–E where the experimental average cell counts of OT-I T cells at 2, 3, 4, 6, and 8 dpi (table S1) are plotted with a simulation run (table S4). In this example, the APC population is rate limiting and allows naïve OT-I T cells (A) to accumulate rapidly over the first 30 hours and then decay exponentially for the remainder of the 8-day period (Fig. 7B). The number of free APCs (P) remains low throughout the simulation as any available APC almost immediately pairs with a naïve OT-I T cell (AP) (Fig. 7C) and converts to a $Nur77^{GFP+}$ OT-I:APC pair (BP). The duration of the BP population is roughly 24 hours to approximate the second phase of DC:T cell interactions during priming (25). The BP trajectory follows the linear decrease of the APC population over time as approximated by the model ($p_{BP,leave}$). Simulation of divisions 1–6 (Fig. 7D–E) reflect the 24-hour T cell priming cycle of BP and the 5.3 hour division cycle (26). The effect of the linear reduction of BP over time is evidenced by the decreasing cell counts in divisions 1–6 (Fig. 7D–E). Division 8+ (J) has a different profile (Fig. 7E), because these cells are all $CTV^-$ and continue dividing (27) making J the sum of all divisions ≥8.

The comparison of simulations of the kinetics of the OT-I T cell response in WT and *Batf3*$^{-/-}$ mice using the STORE model with actual experimental data showed that the number of each T cell division at each time point matched well (Fig. 7F). This evaluation highlighted that the major difference between WT and *Batf3*$^{-/-}$ mice is the probability of OT-I T cells in divisions 3–6 leaving the system by 68 hpi. When OT-I T cells in the omentum were examined for differing rates of cell death at 3 dpi, cells in divisions 3 and 4 showed increased cell death in *Batf3*$^{-/-}$ compared to WT mice (Fig. 7G–H). The blastogenic T cell response requires increased metabolic activity driven by aerobic glycolysis and mitochondrial activity, enhanced responsiveness to IL-2, and nutrient uptake. In OT-I T cells that had become activated and begun to proliferate in WT or *Batf3*$^{-/-}$ mice, there was no difference in mitochondrial mass or surface expression of the glucose uptake receptor Glut1 (fig. S3H–I). UMAP analysis of expression of a panel of T cell activation-dependent receptors and CTV dilution at 3 dpi differentiated between OT-I T cells from WT versus *Batf3*$^{-/-}$ recipients (Fig. 7I). While expression levels of CD69 and CD11a showed little difference between these populations, the nutrient uptake receptors CD71 and CD98, as well

as the cytokine receptor IL-2Rα (CD25), showed increased expression in OT-I cells from WT recipients (Fig. 7J). The expression level of CD71, CD98, and CD25 was significantly higher in divisions 3–6 of OT-I cells in WT mice compared to those from *Batf3*$^{-/-}$ mice (Fig. 7K–P). Together, the agent-based model and experimental data sets indicate that after T cell priming cDC1 promote entry of CD8$^{+}$ T cells into a pro-survival expansion phase, and that the loss of cDC1 resulted in a defect in the expression of nutrient and IL-2 receptors that support the T cell proliferative burst (28, 29).

## DISCUSSION

The importance of WAT and the FALCs located therein to the immune response is appreciated, but reports that FALCs lack organized T and B cell regions, follicular dendritic cells (FDCs), and a central reticular network suggest FALCs are not capable of the same functions as SLOs (7). However, adaptive immune responses thought to occur exclusively in SLOs can be initiated in the omentum (7) and fat-resident memory CD8$^{+}$ T cells benefit from the local metabolic resources (3). Here, we demonstrate cDC1 in FALCs have the same capacity as their counterparts in SLOs to coordinate changes in cellularity associated with ILC activation and monocyte mobilization along with CD8$^{+}$ T cell priming and expansion. These findings illustrate the dynamic nature of the FALCs and highlight them as a site of interactions between the innate and adaptive responses. Given the differences in organization between the SLO and FALCs, what are the features of these lymphoid aggregates that allows them to accomplish the same functions as SLO? First, the placement of FALCs at a serosal surface facilitates the collection of antigens leaving the peritoneum via convective flow or trafficking by immune cells through the stomata in the mesothelium into the FALCs (9, 12). Second, stromal cell chemokine production recruits ILCs to the FALCs (6, 7, 9–11). Third, while tissue-resident macrophages are considered nonmigratory, the macrophages resident in body cavities do not adhere to this principle and can access other tissues (30). This migratory capacity allows these macrophages to deliver antigen to the FALCs. Perhaps, FALCs should be considered as evolutionarily conserved, mesoderm-derived structures that are specialized for surveillance of cavities and are a relevant site for initiation of T- and B-cell-mediated immunity.

The ability of antigen-laden cDC to migrate from tissues to different regions of SLOs is considered critical to initiate and coordinate T cell activation (14). Utilization of Cre-secreting CPS parasites revealed infected peritoneal macrophages that migrate into the FALCs were sufficient for initial priming of the CD8$^{+}$ T cells. This migration of infected macrophages is likely enhanced by parasite effector proteins that promote leukocyte migration (31). This unanticipated conclusion has parallels to studies that examined the events associated with T cell priming following subcutaneous introduction of VV. In that setting, early activation of CD8$^{+}$ T cells was associated with infected macrophages in the subcapsular sinus (SCS) of the draining LN before T cell cluster formation around cDC adjacent to the macrophage-rich zone (32). A subsequent study utilized VV to show that infected cDC populations mediate CD8$^{+}$ T cell priming, and was the only prior study to show that cDC1 in the spleen and LN were not required for this priming (13). The topic of which cell type is involved in the initial presentation of cognate peptide to T cells is complicated. For example, strategies that target antigen to cDC subsets (33) reveal

the function of cDC but do not reflect the biology of different infections. Because many pathogens vary in their cellular tropism and microbial evasion mechanisms that target antigen presentation, it seems likely that multiple mechanisms to allow T cell priming would exist.

A common feature of studies that imaged early cDC:T cell interactions during infection is the observation that “secondary” cluster formation occurs around cDC that were not infected, but it was unclear if cDC that nucleated the clusters had been previously infected or whether they were presenting antigen. The observation that cDC1 enriched in the T cell zone of the MS were associated with clusters of activated OT-I T cells illustrates a process common to FALCs and SLO. The use of the Cre-expressing parasites established that these cDC1 had neither been infected nor injected by the parasites, but the loss of $CD8^+$ T cell responses in the *Xcr1*-β2M mice indicated that these cDC1 present antigen and do not utilize MHC Class I dressing reported in other systems (34, 35). Given the ability of cDC1 to cross-present antigen, it seems likely that uninfected cDC1 acquire antigen secreted from the parasite or released upon death of infected cells. Regardless, these cDC provide a platform to facilitate T cell help (13, 15, 17) and crosstalk between $CD8^+$ T cells (36). How absence of this activity affects T cell proliferation and differentiation is not well understood. The use of differential equations has helped to understand T cell activation, expansion and differentiation pathways (27, 37, 38). However, these deterministic models do not account for stochasticity in biological samples and are poorly suited for the analysis of small numbers of cells or to capture rare events such as initial APC:T cell interactions (39). To better understand how loss of cDC1 impacts T cell expansion, the agent-based STORE model was developed. Importantly, this stochastic model required only a small number of parameters to recapitulate the early *in vivo* response of OT-I T cells and predicted that a loss of cDC1 would lead to an increased rate of cell death of OT-I T cells in their early divisions. This result led to the recognition that early cDC1:$CD8^+$ T cell interactions promote expression of nutrient and cytokine receptors that support T cell proliferation required for the generation of memory $CD8^+$ T cell responses. The development of an accurate stochastic model of early T cell responses provides an opportunity to test how changes in T cell priming impact memory formation and should allow for the directed design of vaccination strategies to elicit a protective cellular immune response.

## MATERIALS AND METHODS

### Study design

This study was designed to understand the role of cDC1 in orchestrating the generation of a protective memory $CD8^+$ T cell population in the FALCs of the omentum in response to vaccination with a non-replicating strain of *T. gondii*. To do so, we primarily compared the immune response to vaccination in WT mice and mice lacking cDC1 (*Batf3*$^{-/-}$ and *Irf8 +32*$^{-/-}$ mice). Measurements of $CD8^+$ T cells at acute and memory time points in these different mouse models demonstrated the importance of cDC1 in generating these populations. The early priming events of $CD8^+$ T cells in the omentum were thus examined and an agent-based model was developed to understand the kinetics and mechanism of these differences. Endpoint analyses included flow cytometry, survival

curves, fluorescence imaging, cluster analysis using K-function statistics, and agent-based modeling. All experiments used randomly assigned mice without investigator blinding. All data points and *n* values reflect biological replicates, and no data was excluded. The specific numbers and genotypes of the mice, the number of replicates, and the statistics performed are included in the legend of each figure.

## Mice

All procedures involving mice were reviewed and approved by the Institutional Animal Care and Use Committee of the University of Pennsylvania (Animal Welfare Assurance Reference Number #A3079-01) and were in accordance with the guidelines set forth in the Guide for the Care and Use of Laboratory Animals of the National Institute of Health.

*Batf3*$^{-/-}$ (Stock #013755, RRID:IMSR_JAX:013755), *Il12b*$^{-/-}$ (Stock #002693, RRID:IMSR_JAX:002693), Ai6 (Stock #007906, RRID:IMSR_JAX:007906), Nur77$^{GFP}$ (Stock #016617, RRID:IMSR_JAX:016617), OT-I (Stock #003831, RRID:IMSR_JAX:003831), *Irf8 +32*$^{-/-}$ (Stock #032744, RRID:IMSR_JAX:032744), Rag1$^{-/-}$ (Stock #002216, RRID:IMSR_JAX:002216), and *Lyz2*-Cre (Stock #004781, RRID:IMSR_JAX:004781) mice were obtained from Jackson Laboratories. C57BL/6 (Stock #B6-F/M) and Rag2$^{-/-}\gamma c^{-/-}$ (Stock #4111) mice were obtained from Taconic Biosciences (RRID:SCR_016410). CD45.1 (Stock #564) mice were obtained from Charles River Laboratories. *Snx22*$^{GFP/+}$ mice (on a 129S1 background) were produced by standard homologous recombination in ES cells (54), and were a kind gift from Dr. Kenneth M. Murphy at Washington University in St. Louis. *Snx22*$^{GFP/+}$ mice used here were an F1 cross with C57BL/6 mice. *Xcr1*-Cre mice were generated previously (30) and were a kind gift from Dr. Kenneth M. Murphy at Washington University in St. Louis. Floxed β2-microglobulin mice were obtained from Dr. Dorian B. McGavern at the NIH in Bethesda. All mice are on a C57BL/6 background unless otherwise noted. For IL-12p70 add back experiments, C57BL/6 and *Batf3*$^{-/-}$ mice were treated with an intraperitoneal (i.p.) injection of either PBS (Corning: 21-0311-CM) or 200 ng of recombinant murine IL-12p70 (PeproTech: 210-12) immediately after immunization and once per day for the next two days after immunization. All mice were kept in specific-pathogen-free conditions at the School of Veterinary Medicine at the University of Pennsylvania.

## Immunizations and infections

All *Toxoplasma gondii* immunizations were performed using 1–2 × $10^5$ *cpsII* parasites, *cpsII*-OVA parasites, or *cpsII*-Cre-OVA-mCherry parasites. Infectious challenge experiments were performed using $10^4$ *Pru*-OVA parasites or RH parasites. *CpsII*-OVA parasites have been previously described (36) and were derived from the RHΔ*cpsII* clone, which was provided as a generous gift by Dr. David Bzik. *CpsII*-Cre-OVA-mCherry parasites were derived from the *cpsII*-OVA clone using the previously described methods (36, 43). *Pru*-OVA parasites have also been described previously (36). Parasites were cultured and maintained by serial passage on human foreskin fibroblast cells in the presence of parasite culture media [71.7% DMEM (Corning: 10-017-CM), 17.9% Medium 199 (Gibco: 11150-059), 9.9% Fetal Bovine Serum (FBS)(Atlanta Biologics: S11150H), 0.45% Penicillin and Streptomycin (Gibco: 15140-122)(final concentration of 0.05 units/ml

penicillin and 50 μg/ml streptomycin), 0.04% gentamicin (Gibco: 15750-060)(final concentration of 0.02 mg/ml gentamicin)], which was supplemented with uracil (Sigma-Aldrich: U1128) (final concentration of 0.2 mM uracil). For infections, parasites were harvested and serially passed through 18 and 26 gauge needles (BD: 305196, 305115) before filtration with a 5 μM filter (PALL Acrodisc: 4650). Parasites were washed extensively with PBS and mice were injected i.p. with parasites suspended in PBS.

## T cell transfers and tissue harvesting

For T cell transfers OT-I mice were interbred with CD45.1/Nur77$^{GFP}$ mice or CD45.1 mice. To isolate OT-I or P14 CD8$^+$ T cells, lymph nodes and spleen were harvested and leukocytes from the spleen and draining lymph nodes were obtained by processing spleens and lymph nodes over a 70 μm filter (Fisher Scientific: 22-363-548) and washing them in complete RPMI [90% RMPI 1640 (Corning: 10-040-CM), 10% FBS, 1% penicillin-streptomycin, 1 mM sodium pyruvate (Corning: 25-000-Cl), 1% nonessential amino acids (Gibco: 11140-050), and 0.1% β-mercaptoethanol (Gibco: 21985-023)]. Red blood cells were then lysed by incubating for 5 minutes at room temperature in 5 ml of lysis buffer [0.864% ammonium chloride (Sigma-Aldrich: A0171) diluted in sterile de-ionized $H_2O$)], followed by washing with complete RPMI. For transfer of low numbers of OT-I CD8$^+$ T cells, splenocytes were rinsed with PBS and total splenocytes containing $5 \times 10^3$ or $5 \times 10^4$ OT-I T cells were transferred by i.v. injection into recipient mice. For the transfer of high numbers of OT-I CD8$^+$ T cells, cells were then purified by magnetic activated cell sorting (MACS) using the CD8a+ T Cell Isolation Kit (Miltenyi Biotec: 130-104-075). For cell division or microscopy studies, purified OT-I or P14 T cells were then fluorescently labeled using the CellTrace Violet (CTV, ThermoFisher Scientific: C34557) or CellTrace Yellow (CTY, ThermoFisher Scientific: C34567) labeling kits. OT-I T cells were then transferred by either i.v. or i.p. injection into recipient mice.

For the transfer of memory OT-I T cells, total splenocytes containing $5 \times 10^4$ WT CD45.1$^+$ OT-I T cells were i.v. transferred into *Batf3*$^{-/-}$ mice and total splenocytes containing $5 \times 10^4$ WT CD45.1.2$^+$ OT-I T cells were i.v. transferred into WT mice 1 day prior to immunization with $2 \times 10^5$ CPS-OVA parasites. At 42 dpi, spleens from WT and *Batf3*$^{-/-}$ hosts were harvested and processed as above. Single cell suspensions from mice of each host genotype were then pooled and resuspended in sterile FACS buffer. OT-I T cells from WT and *Batf3*$^{-/-}$ hosts were then FACS purified and mixed 1:1 for the i.v. transfer of $2 \times 10^4$ total OT-I T cells into naïve WT mice. These recipient WT mice were then infected i.p. 24 hours later with $10^4$ *Pru*-OVA tachyzoites.

Peritoneal exudate cells were obtained by peritoneal lavage with 8 mL of ice cold PBS. Omentum was isolated, incubated in 0.4 U/mL of LiberaseTL (Roche: 5401020001) for one hour at 37°C, passed through an 18G needle, and processed over a 70 μm filter. Leukocytes from the spleen and draining lymph nodes were obtained by processing spleens and lymph nodes, washing them in complete media, and lysing red blood cells (see above). Cells were then resuspended in complete RPMI.

### T cell priming *in vitro*

For *in vitro* assays measuring priming of naïve $CD8^+$ T cells by infected macrophages, Ai6 mice were immunized i.p. with $5 \times 10^5$ CPS-Cre-OVA-mCherry parasites. At 18 hpi, peritoneal exudate cells were harvested from naïve or immunized Ai6 mice. Large peritoneal macrophages (LPM) were then FACS purified after double sorting to isolate naïve LPM from naïve Ai6 mice or uninfected ($ZsGreen^-$) and infected ($ZsGreen^+$) LPM from 5 different immunized Ai6 mice. These purified populations were then plated in a 96-well plate at $5 \times 10^3$ cells per well. Naïve OT-I/$Nur77^{GFP}$ T cells that had been MACS purified and labeled with CTV were then added at $4 \times 10^4$ cells per well to each well containing LPM. OT-I/$Nur77^{GFP}$ T cell activation was then measured 72 hours later.

### Omentectomy surgeries

The surgical removal of the omentum was performed using standard aseptic technique. Prior to surgery, hair was removed from the ventral side of mice and a single dose of 0.1 mg/kg of buprenorphine was administered by i.p. injection. Mice were then sedated using isoflurane in an induction box, and anesthesia was maintained with a face mask with a constant flow of 1–2% isoflurane. Mice were then placed on a sterile surgical cloth covering a heating pad to provide heat support. The surgical site was then cleaned using a chlorhexidine wipe. A suprapubic midline laparotomy was performed to visualize and expose the omentum. The omentum was then removed using a cauterization pen to sever the connective tissue and blood vessel at each end of the omentum. For sham surgeries, an abdominal incision was made and the omentum was exposed but not removed. The peritoneal wall was closed using 5-0 synthetic absorbable sutures, and the overlaying skin was closed using the same sutures as well as surgical glue. The mice were observed and allowed to recover in a clean cage with a heating pad beneath for heat support until resuming normal activity. Buprenorphine was given to all mice postoperatively at 0.1 mg/kg every 4 hours via subcutaneous injection for the first 48 hours after surgery. Animals were monitored to assess for signs of pain or discomfort and wounds were examined for signs of infection every day for the remainder of the experiment.

### Intravital imaging

Ai6 mice were immunized i.p. with $10^5$ CPS-Cre-OVA-mCherry parasites, and 18 hours later $2 \times 10^5$ naïve, CTV-labeled OT-I/$Nur77^{GFP}$ T cells and $2 \times 10^5$ naïve, CTY-labeled P14 T cells were transferred via i.p. injection. Starting 2 hours later, recipient Ai6 mice were anesthetized with isoflurane and maintained at a core temperature of 37°C. The peritoneum was surgically opened to access the omentum, and a small portion of visceral adipose tissue was resected to assist in immobilizing the omentum via a soft-tissue vacuum apparatus (VueBio). No greater than 40 kPa of pressure was applied to steady the omentum for imaging. Image acquisition was performed on a Leica SP8 multiphoton confocal with a 20X water immersion objective (1.0 NA) with resonant scanner (8000 kHz) and 4 external HyD detectors. The excitation wavelength of Chameleon Vision II Ti:Sapphire laser was tuned for optimal detection of the labeled OT-I and P14 T cells in each experiment, typically 880 nm. Images collected x-, y-, and z-plane data over time with a step size of 2 μm and a z-thickness that allowed for a complete z-series every 22s. This was carried out for approximately

30 minutes for each region imaged. Resulting images were segmented in Imaris (v9.7.2, Bitplane) with spot-specific position data exported and analyzed in R with the CellTrackR package.

## Flow cytometry

Cells were washed with FACS buffer [1× PBS, 0.2% bovine serum antigen (Gemini: 700-100P), 1 mM EDTA (Gibco: 15575-038)] and incubated in Fc block [99.5% FACS Buffer, 0.5% normal rat IgG (Invitrogen: 10700), 1 μg/ml 2.4G2 (BioXCell: BE0307)] at 4°C for 10 min prior to staining. If cells were stained for cell death using LIVE/DEAD staining, LIVE/DEAD Fixable Aqua Dead Cell marker (Invitrogen: L34957), GhostDye Violet 510 Viability Dye (TONBO Biosciences: 13-0870-T100), or GhostDye Red 780 Viability Dye (TONBO Biosciences: 13-0865-T100) was included during incubation with Fc block. Tetramer-specific $CD8^+$ and $CD4^+$ T cells were measured by staining in 50 μL FACS buffer containing MHCI and MHCII tetramers specific for endogenous *T. gondii* antigens for 1 hour at room temperature. Cells were surface stained in 50 μL at 4°C for 15–20 min and washed in FACS buffer prior to acquisition. For intracellular cytokine staining, $10^6$ cells from the peritoneal exudate or omentum were plated in a 96-well plate and incubated with 1X Brefeldin A (Sigma-Aldrich: B7651) at 37°C for 3 hr. For intracellular cytokine and transcription factor staining, cells were rinsed with FACS buffer and surface stained as described above, fixed using the eBioscience Foxp3 Transcription Factor Fixation/ Permeabilization Concentrate and Diluent (ThermoFisher Scientific: 00-8222) for 30 min at 4°C, and then washed with FACS buffer. Cells were then stained for intracellular cytokines and transcription factors in 50 μL 1X eBioscience Permeabilization Buffer (ThermoFisher Scientific: 00-8333-56) at 4°C for at least 1 hr. Cells were then washed in FACS buffer prior to acquisition. The APC Annexin V Kit (BioLegend: 640920) was used to measure cell death via Annexin V and propidium iodide (PI). Cells were surface stained and washed with FACS buffer then resuspended in 100 μL Annexin V binding buffer (BioLegend: 79998). Cells were then incubated with 5 μL APC Annexin V (BioLegend: 640920) and 10 μL PI solution (BioLegend: 79997) for 15 min at room temperature in the dark. Prior to acquisition, 400 μL of Annexin V binding buffer was added to each sample. For mitochondrial staining $2 \times 10^6$ cells were suspended in 100 μL HBSS (Gibco: 14175-079) supplemented with 0.5 mM $MgCl_2$ (Sigma-Aldrich: M4880). Mitochondrial stains were then added at the following concentrations: 50 nM MitoTracker Green FM (Invitrogen: M7514), 25 nM MitoTracker Deep Red FM (Invitrogen: M22426) and 5 mM MitoSOX Red (Invitrogen: M36008). Samples were incubated at 37°C for 30 min, rinsed with FACS buffer, and surface stained as above prior to acquisition.

The following antibodies were used for staining: B220: BV510, BioLegend: 103248, clone: RA3-6B2, RRID:AB_2650679; B220: ef450, eBioscience: 48-0452-82, clone: RA3-6B2, RRID:AB_1548761; B220: PerCp-Cy5.5, BioLegend: 103236, clone: RA3-6B2, RRID:AB_893356; CCR2: AF647, BioLegend: 150604, clone: SA203G11, RRID:AB_2566140; CD102: BUV395, BD Biosciences: 740227, clone: 3C4 (mIC2/4), RRID:AB_2739975; CD102: ef450, eBioscience: 48-1021-82, clone: 3C4 (mIC2/4), RRID:AB_1548749; CD102: FITC, BioLegend: 105606, clone: 3C4 (mIC2/4), RRID:AB_313199; CD115: BV605, BioLegend: 135517,

clone: AF398, RRID:AB_2562760; CD11a: PerCp-Cy5.5, BioLegend: 101124, clone: M17/4, RRID:AB_2562932; CD11b: APC-ef780, eBioscience: 47-0112-82, clone: M1/70, RRID:AB_1603193; CD11b: BV605, BioLegend: 101257, clone: M1/70, RRID:AB_2565431; CD11b: BV650, BioLegend: 101259, clone: M1/70, RRID:AB_2566568; CD11c: APC-Fire750, BioLegend: 117352, clone: N418, RRID:AB_2572124; CD11c: APC-R700, BD Biosciences: 565872, clone: N418, RRID:AB_2744277; CD11c: BUV737, BD Biosciences: 612797, clone: HL3, RRID:AB_2870124; CD172a: APC, BioLegend: 144014, clone: P84, RRID:AB_2564061; CD172a: APC-Cy7, BioLegend: 144018, clone: P84, RRID:AB_2629558; CD19: BV605, BioLegend: 115539, clone: 6D5, RRID:AB_11203538; CD19: ef450, eBioscience: 48-0193-82, clone: eBio1D3, RRID:AB_2734905; CD19: PerCp-Cy5.5, BioLegend: 152406, clone: ID3/CD19, RRID:AB_2629815; CD200R: APC, eBioscience: 17-5201-82, clone: OX110, RRID:AB_10717289; CD25: APC, eBioscience: 17-0251-82, clone: PC61.5, RRID:AB_469366; CD25: PE-Cy7, eBioscience: 25-0251-82, clone: PC61.5, RRID:AB_469608; CD3: APC-ef780, Invitrogen: 47-0032-82, clone: 17A2, RRID:AB_1272181; CD3: BV605, BioLegend: 100237, clone: 17A2, RRID:AB_2562039; CD3: BV750, BioLegend: 100249, clone: 17A2, RRID:AB_2734148; CD3: BV785, BioLegend: 100232, clone: 17A2, RRID:AB_2562554; CD3: PacBlue, BioLegend: 100214, clone: 17A2, RRID:AB_493645; CD3e: PE-cf594, BD Biosciences: 562286, clone: 145-2C11, RRID:AB_11153307; CD3e: PerCp-Cy5.5, Invitrogen: 45-0031-82, clone: 145-2C11, RRID:AB_1107000; CD335: BV650, BioLegend: 137635, clone: 29A1.4, RRID:AB_2734200; CD335: PE-Dazzle594, BioLegend: 137630, clone: 29A1.4, RRID:AB_2616666; CD4: AF700, BioLegend: 100536, clone: RM4-5, RRID:AB_493701; CD4: BV650, BioLegend: 100555, clone: RM4-5, RRID:AB_2562529; CD4: BV711, BioLegend: 100447, clone: GK1.5, RRID:AB_2564586; CD4: BV785, BioLegend: 100552, clone: RM4-5, RRID:AB_2563053; CD44: BV605, BD Biosciences: 563058, clone: IM7, RRID:AB_2737979; CD44: BV785, BioLegend: 103059, clone: IM7, RRID:AB_2571953; CD45: BUV805, BD Biosciences: 748370, clone: 30-F11, RRID:AB_2872789; CD45.1: APC-ef780, Invitrogen: 47-0453-82, clone: A20, RRID:AB_1582228; CD45.1: BV711, BioLegend: 110739, clone: A20, RRID:AB_2562605; CD45.1: ef450, Invitrogen: 48-0453-82, clone: A20, RRID:AB_1272189; CD45.1: PE, BD Biosciences: 553776, clone: A20, RRID:AB_395044; CD45.1: PE-cf594, BD Biosciences: 562452, clone: A20, RRID:AB_11152958; CD45.1: PerCp-Cy5.5, Invitrogen: 45-0453-82, clone: A20, RRID:AB_1107003; CD45.2: APC-ef780, Invitrogen: 47-0454-82, clone: 104, RRID:AB_1272175; CD45.2: BV711, BioLegend: 109847, clone: 104, RRID:AB_2616859; CD49b: FITC, BD Biosciences: 553857, clone: DX5, RRID:AB_395093; CD5: ef450, eBioscience: 48-0051-82, clone: 53-7.3, RRID:AB_1603250; CD5: PerCp-Cy5.5, eBioscience: 45-0051-82, clone: 53-7.3, RRID:AB_914334; CD62L: APC-ef780, eBioscience: 47-0621-82, clone: MEL-14, RRID:AB_1603256; CD62L: BV711, BioLegend: 104445, clone: MEL-14, RRID:AB_2564215; CD64: PE-Cy7, BioLegend: 139314, clone: X54-5/7.1, RRID:AB_2563904; CD69: BV711, BioLegend: 104537, clone: H1.2F3, RRID:AB_2566120; CD69: ef450, Invitrogen: 48-0691-82, clone: H1.2F3, RRID:AB_10719430; CD69: PE-Cy7, BD Biosciences: 552879, clone: H1.2F3, RRID:AB_394508; CD69: PerCp-Cy5.5, eBioscience: 45-0691-82, clone: H1.2F3, RRID:AB_1210703; CD71: PE, BioLegend: 113807, clone: R17217,

RRID:AB_313568; CD8a: BV605, BioLegend: 100744, clone: 53-6.7, RRID:AB_2562609; CD8a: BV650, BioLegend: 100742, clone: 53-6.7, RRID:AB_2563056; CD8a: BV711, BioLegend: 100747, clone: 53-6.7, RRID:AB_11219594; CD8b: APC-ef780, Invitrogen: 47-0083-82, clone: ebioH35-17.2, RRID:AB_2573943; CD8b: FITC, BioLegend: 126606, clone: YTS156.7.7, RRID:AB_961295; CD90.2: AF700, BioLegend: 105320, clone: 30-H12, RRID:AB_493725; CD98: PE-Cy7, BioLegend: 128214, clone: RL388, RRID:AB_2750547; CD117/c-kit: APC-ef780, Invitrogen: 47-1172-80, clone: ACK2, RRID:AB_1582227; CXCR3: BV650, BioLegend: 126531, clone: CXCR3-173, RRID:AB_2563160; CXCR3: PE-Cy7, BioLegend: 126516, clone: CXCR3-173, RRID:AB_2245493; EOMES: PE, Invitrogen: 12-4875-80, clone: Dan11mag, RRID:AB_1603278; F4/80: ef450, Invitrogen: 48-4801-80, clone: BM8, RRID:AB_1548756; FcεR1a: APC, Invitrogen: 17-5898-82, clone: 1-Mar, RRID:AB_10718824; Glut1: AF647, AbCam: ab195020, clone: EPR3915, RRID:AB_2783877; I-A/I-E: AF700, BioLegend: 107622, clone: M5/144.15.2, RRID:AB_493727; I-A/I-E: BV711, BioLegend: 107643, clone: M5/144.15.2, RRID:AB_2565976; IFN-γ: PE-Cy7, Invitrogen: 25-7311-82, clone: XMG1.2, RRID:AB_469680; KLRG1: BV711, BioLegend: 138427, clone: 2F1/KLRG1, RRID:AB_2629721; KLRG1: FITC, eBioscience: 11-5893-82, clone: 2F1, RRID:AB_1311265; LFA1: PerCp-Cy5.5, BioLegend: 141008, clone: H155-78, RRID:AB_1311265; Ly6C: BV570, BioLegend: 128030, clone: HK1.4, RRID:AB_2562617; Ly6C: BV785, BioLegend: 128041, clone: HK1.4, RRID:AB_2565852; Ly6G: BUV563, BD Biosciences: 612921, clone: 1A8, RRID:AB_2870206; Ly6G: PE, BioLegend: 127608, clone: 1A8, RRID:AB_1186099; NK1.1: BV711, BioLegend: 108745, clone: PK136, RRID:AB_2563286; NK1.1: PerCp-Cy5.5, BioLegend: 108728, clone: PK136, RRID:AB_2132705; SiglecF: PE, BD Biosciences: 552126, clone: E50-2440, RRID:AB_394341; SiglecH: BV421, BD Biosciences: 566581, clone: 440C, RRID:AB_2739747; TCR Vα2: PE, BioLegend: 127808, clone: B20.1, RRID:AB_1134183; TCR Vα2: Superbright780, Invitrogen: 78-5812-82, clone: B20.1, RRID:AB_2735086; TCR Vβ5.1,5.2: APC, BioLegend: 139506, clone: MR9-4, RRID:AB_10933250; TCRβ: PerCp-Cy5.5, BioLegend: 109228, clone: H57-597, RRID:AB_1575173; Tetramer MHCI: PE, NIH Tetramer Core, peptide: SVLAFRRL; Tetramer MHCII: PE, NIH Tetramer Core, peptide: AVEIHRPVPGTAPPS; Tetramer MHCI: APC, NIH Tetramer Core, peptide: SVLAFRRL; Tetramer MHCII: APC, NIH Tetramer Core, peptide: AVEIHRPVPGTAPPS; XCR1: BV650, BioLegend: 148220, clone: ZET, RRID:AB_2566410; XCR1: BV785, BioLegend: 148225, clone: ZET, RRID:AB_2783119; TCF1: AF488, Cell Signaling: 6444S, clone: C63D9, RRID:AB_2797627; Tbet: AF647, BioLegend: 644804, clone: 4B10, RRID:AB_1595466; CD86: AF700, BioLegend: 105024, clone: GL-1, RRID:AB_493721; Ki67: AF700, BD Biosciences: 561277, clone: B56, RRID:AB_10611571; CD45.1: APC, eBioscience: 17-0453-82, clone: A20, RRID:AB_469398; CD64: APC, BioLegend: 139306, clone: X54-5/7.1, RRID:AB_11219391; CD8β: APC, BioLegend: 126614, clone: YTS156.7.7, RRID:AB_2562775; CD44: APC-Cy7, BioLegend: 103028, clone: IM7, RRID:AB_830785; F4/80: APC-ef780, eBioscience: 47-4801-82, clone: BM8, RRID:AB_2735036; Ly6C: APC-ef780, eBioscience: 47-5932-82, clone: HK1.4, RRID:AB_2573992; KLRG1: BUV395, BD Biosciences: 740279, clone: 2F1, RRID:AB_2740018; CD4: BUV496,

BD Biosciences: 612952, clone: GK1.5, RRID:AB_2813886; CD8α: BUV563, BD Biosciences: 748535, clone: 53-6.7, RRID:AB_2872946; CD11b: BUV661, BD Biosciences: 565080, clone: M1/70, RRID:AB_2722548; CD122: BUV661, BD Biosciences: 741493, clone: TM-β1, RRID:AB_2870951; CD19: BUV661, BD Biosciences: 612971, clone: 1D3, RRID:AB_2870243; CD11a: BUV805, BD Biosciences: 741919, clone: 2D7, RRID:AB_2871232; CD8α: BUV805, BD Biosciences: 612898, clone: 53-6.7, RRID:AB_2870186; CD127: BV421, BioLegend: 135027, clone: A7R34, RRID:AB_2563103; CD19: BV421, BioLegend: 115538, clone: 6D5, RRID:AB_11203527; CXCR3: BV421, BioLegend: 126529, clone: CXCR3-173, RRID:AB_2563100; CD43: BV605, BD Biosciences: 747726, clone: S7, RRID:AB_2872201; CD62L: BV605, BioLegend: 104437, clone: MEL-14, RRID:AB_11125577; CD19: BV650, BioLegend: 115541, clone: 6D5, RRID:AB_11204087; CD27: BV650, BioLegend: 124233, clone: LG.3A10, RRID:AB_2687192; CX3CR1: BV785, BioLegend: 149029, clone: SA011F11, RRID:AB_2565938; CD122: FITC, BioLegend: 123207, clone TM-β1, RRID:AB_940611; CD80: FITC, eBioscience: 11-0801-85, clone: 16-10A1, RRID:AB_465134; β2-microglobulin: PE, BioLegend: 154504, clone: A16041A, RRID:AB_2721340; CD212: PE, BD Biosciences: 551974, clone: 114, RRID:AB_394310; CD127: PE-Cy7, BioLegend: 135014, clone: A7R34, RRID:AB_1937265; CD71: PerCp-Cy5.5, BioLegend: 113816, clone: R17217, RRID:AB_2565482; CX3CR1: PerCp-Cy5.5, BioLegend: 149009, clone: SA011F11, RRID:AB_2564493; CD8β: PerCp-ef710, Invitrogen: 46-0083-82, clone: ebioH35-17.2, RRID:AB_10669709.

Samples were run on a LSR Fortessa (BD), LSRII (BD), FACSymphony A3 (BD), or FACSymphony A5 (BD) and analyzed using FlowJo Software (TreeStar).

## Immunofluorescence imaging

Whole omenta were harvested from mice and fixed in 1% PFA overnight at 4°C. After rinsing, tissue was blocked using 10% BSA, 0.5% normal rat serum (Invitrogen), and 1 μg/ml 2.4G2 (BD) in PBS for 1 hr at room temperature. For immunofluorescence staining, omenta were incubated in PBS containing primary antibodies at 4°C for 3 days and subsequently rinsed with PBS overnight. Antibodies included: B220: AF647, BD Biosciences: 557683, clone: RA3-6B2; B220: BV510, BioLegend: 103248, clone: RA3-6B2; CD11b: AF700, eBioscience: 56-0112-82, clone: M1/70; CD3: AF532, Invitrogen: 58-0032-82, clone: 17A2; CD4: AF532, Invitrogen: 58-0042-82, clone: RM4-5; CD8b: ef450, Invitrogen: 48-0082-82, clone: eBioH35-17.2; ER-TR7: AF647, Santa Cruz Biotechnology: sc-73355 AF647, clone: ER-TR7. Tissues were then mounted on slides using Prolong Diamond (Invitrogen: P36970) or Prolong Glass mounting media (Invitrogen: P36984) and imaged using a Leica TCS SP8 STED microscope and acquired using LAS X (Leica Microsystems). Images were processed and analyzed using LAS X and Imaris (Oxford Instruments).

## Cluster analysis

Clustering was analyzed using K function statistics as described in full in Appendix C. Briefly, to determine clustering of $Nur77^{GFP+}$ OT-I T cells, the average number of $Nur77^{GFP+}$ cells within a specified distance, *k*, of each $Nur77^{GFP+}$ cell was compared

with those averages calculated for 999 randomly permuted patterns of the full population of both Nur77$^{GFP+}$ and Nur77$^{GFP-}$ cells. The subpopulation of Nur77$^{GFP+}$ cells was then deemed to be significantly clustered at scale $k$ if the fraction of patterns with averages as large as the observed pattern was not greater than 0.05. To determine whether Nur77$^{GFP+}$ cells were clustered around a specific APC population, the target population is deemed to be significantly clustered around the reference population at scale $k$ if the fraction of randomly permuted populations with an average number of target cells with $k$ as large as the observed population is not larger than 0.05. Similarly, the target population is deemed to be significantly dispersed away from the reference population at scale $k$ if the fraction of populations with averages as small as the observed population is not larger than 0.05.

### STochastic Omentum REsponse (STORE) model

The STORE model is a dynamic stochastic mathematical model used to simulate the early OT-I T cell response to immunization in the omentum and is described in full in the Supplementary Methods. Briefly, the model is based off experimental data measuring the kinetics of the OT-I T cell response in the omentum through the first 8 days of immunization. Simulations of the model track the interactions of transferred OT-I T cells with APC populations and the subsequent T cell divisions that drive the expansion of the OT-I T cell population. The behavior of every cell within the system is tracked individually throughout the simulation and is determined by probability distributions estimated from the literature or taken as a separate parameter. The goal of the model is to recapitulate the experimental data for OT-I T cells with the tabulated parameters defining the differences between the responses of OT-I T cells in the WT and *Batf3*$^{-/-}$ mice.

### Statistical analysis

Statistical analysis was performed using GraphPad PRISM 9.0 software. The statistical analysis and significance values for each comparison are indicated in each figure caption.

## Supplementary Material

Refer to Web version on PubMed Central for supplementary material.

## ACKNOWLEDGMENTS

We would like to acknowledge the contributions of Andrea Stout, PhD and the Cell and Developmental Biology Microscopy Core at the Perelman School of Medicine, University of Pennsylvania. We would also like to acknowledge the contributions of the Penn Vet Imaging Core at the University of Pennsylvania School of Veterinary Medicine.

### FUNDING

This work was supported by grants from the National Institutes of Health: NIAID AI126899-01 RO1/UO1, NIAID 1R21AI126042-01, NIAID R01AI125563, and NIAID AI160664-01 U01.

## DATA AND MATERIALS AVAILABILITY

All data needed to evaluate the conclusions in the paper are present in the paper or the Supplementary Materials. Requests for materials should be directed to the corresponding author.

## REFERENCES AND NOTES


1. Bénézech C, Luu N-T, Walker JA, Kruglov AA, Loo Y, Nakamura K, Zhang Y, Nayar S, Jones LH, Flores-Langarica A, McIntosh A, Marshall J, Barone F, Besra G, Miles K, Allen JE, Gray M, Kollias G, Cunningham AF, Withers DR, Toellner KM, Jones ND, Veldhoen M, Nedospasov SA, McKenzie ANJ, Caamaño JH, Inflammation-induced formation of fat-associated lymphoid clusters, Nat. Immunol 16, 819–828 (2015). [PubMed: 26147686]
2. Moro K, Yamada T, Tanabe M, Takeuchi T, Ikawa T, Kawamoto H, Furusawa J, Ohtani M, Fujii H, Koyasu S, Innate production of TH2 cytokines by adipose tissue-associated c-Kit+Sca-1+ lymphoid cells, Nature 463, 540–544 (2009). [PubMed: 20023630]
3. Han S-J, Zaretsky AG, Andrade-Oliveira V, Collins N, Dzutsev A, Shaik J, da Fonseca DM, Harrison OJ, Tamoutounour S, Byrd AL, Smelkinson M, Bouladoux N, Bliska JB, Brenchley JM, Brodsky IE, Belkaid Y, White Adipose Tissue Is a Reservoir for Memory T Cells and Promotes Protective Memory Responses to Infection, Immunity 47, 1154–1168.e6 (2017). [PubMed: 29221731]
4. Jackson-Jones LH, Duncan SM, Magalhaes MS, Campbell SM, Maizels RM, McSorley HJ, Allen JE, Bénézech C, Fat-associated lymphoid clusters control local IgM secretion during pleural infection and lung inflammation, Nat. Commun 7, 12651 (2016). [PubMed: 27582256]
5. Buscher K, Wang H, Zhang X, Striewski P, Wirth B, Saggu G, Lütke-Enking S, Mayadas TN, Ley K, Sorokin L, Song J, Protection from septic peritonitis by rapid neutrophil recruitment through omental high endothelial venules, Nat. Commun 7, 10828 (2016). [PubMed: 26940548]
6. Jackson-Jones LH, Smith P, Portman JR, Magalhaes MS, Mylonas KJ, Vermeren MM, Nixon M, Henderson BEP, Dobie R, Vermeren S, Denby L, Henderson NC, Mole DJ, Bénézech C, Stromal Cells Covering Omental Fat-Associated Lymphoid Clusters Trigger Formation of Neutrophil Aggregates to Capture Peritoneal Contaminants, Immunity 52, 700–715.e6 (2020). [PubMed: 32294409]
7. Rangel-Moreno J, Moyron-Quiroz JE, Carragher DM, Kusser K, Hartson L, Moquin A, Randall TD, Omental Milky Spots Develop in the Absence of Lymphoid Tissue-Inducer Cells and Support B and T Cell Responses to Peritoneal Antigens, Immunity 30, 731–743 (2009). [PubMed: 19427241]
8. Meza-Perez S, Randall TD, Immunological Functions of the Omentum, Trends Immunol. 38, 526–536 (2017). [PubMed: 28579319]
9. Berberich S, Dahne S, Schippers A, Peters T, Müller W, Kremmer E, Forster R, Pabst O, Differential Molecular and Anatomical Basis for B Cell Migration into the Peritoneal Cavity and Omental Milky Spots, J. Immunol 180, 2196–2203 (2008). [PubMed: 18250426]
10. Perez-Shibayama C, Gil-Cruz C, Cheng H-W, Onder L, Printz A, Mörbe U, Novkovic M, Li C, Lopez-Macias C, Buechler MB, Turley SJ, Mack M, Soneson C, Robinson MD, Scandella E, Gommerman J, Ludewig B, Fibroblastic reticular cells initiate immune responses in visceral adipose tissues and secure peritoneal immunity, Sci. Immunol 3, eaar4539 (2018).
11. Carlow DA, Gold MR, Ziltener HJ, Lymphocytes in the Peritoneum Home to the Omentum and Are Activated by Resident Dendritic Cells, J. Immunol 183, 1155–1165 (2009). [PubMed: 19553538]
12. Sarfarazi A, Lee G, Mirjalili SA, Phillips ARJ, Windsor JA, Trevaskis NL, Therapeutic delivery to the peritoneal lymphatics: Current understanding, potential treatment benefits and future prospects, Int. J. Pharm 567, 118456 (2019). [PubMed: 31238102]
13. Eickhoff S, Brewitz A, Gerner MY, Klauschen F, Komander K, Hemmi H, Garbi N, Kaisho T, Germain RN, Kastenmüller W, Robust Anti-viral Immunity Requires Multiple Distinct T Cell-Dendritic Cell Interactions, Cell 162, 1322–1337 (2015). [PubMed: 26296422]
14. Eisenbarth SC, Dendritic cell subsets in T cell programming: location dictates function, Nat. Rev. Immunol 19, 89–103 (2018).
15. Hor JL, Whitney PG, Zaid A, Brooks AG, Heath WR, Mueller SN, Spatiotemporally Distinct Interactions with Dendritic Cell Subsets Facilitates CD4+ and CD8+ T Cell Activation to Localized Viral Infection, Immunity 43, 554–565 (2015). [PubMed: 26297566]
16. Theisen DJ, DavidsonIV JT, Briseño CG, Gargaro M, Lauron EJ, Wang Q, Desai P, Durai V, Bagadia P, Brickner JR, Beatty WL, Virgin HW, Gillanders WE, Mosammaparast N, Diamond

MS, Sibley LD, Yokoyama W, Schreiber RD, Murphy TL, Murphy KM, WDFY4 is required for cross-presentation in response to viral and tumor antigens, Science 362, 694–699 (2018). [PubMed: 30409884]

17. Ferris ST, Durai V, Wu R, Theisen DJ, Ward JP, Bern MD, Davidson JT, Bagadia P, Liu T, Briseño CG, Li L, Gillanders WE, Wu GF, Yokoyama WM, Murphy TL, Schreiber RD, Murphy KM, cDC1 prime and are licensed by CD4+ T cells to induce anti-tumour immunity, Nature 584, 624–629 (2020). [PubMed: 32788723]
18. Dupont CD, Christian DA, Selleck EM, Pepper M, Leney-Greene M, Pritchard GH, Koshy AA, Wagage S, Reuter MA, Sibley LD, Betts MR, Hunter CA, Parasite Fate and Involvement of Infected Cells in the Induction of CD4+ and CD8+ T Cell Responses to Toxoplasma gondii, PLoS Pathog. 10, e1004047 (2014). [PubMed: 24722202]
19. Shah S, Grotenbreg GM, Rivera A, Yap GS, An extrafollicular pathway for the generation of effector CD8+ T cells driven by the proinflammatory cytokine, IL-12, eLife 4, e09017 (2015). [PubMed: 26244629]
20. Christian DA, Koshy AA, Reuter MA, Betts MR, Boothroyd JC, Hunter CA, Use of Transgenic Parasites and Host Reporters To Dissect Events That Promote Interleukin-12 Production during Toxoplasmosis, Infect. Immun 82, 4056–4067 (2014). [PubMed: 25024368]
21. Koshy AA, Dietrich HK, Christian DA, Melehani JH, Shastri AJ, Hunter CA, Boothroyd JC, Toxoplasma Co-opts Host Cells It Does Not Invade, PLoS Pathog. 8, e1002825 (2012). [PubMed: 22910631]
22. Yarovinsky F, Innate immunity to Toxoplasma gondii infection, Nat. Rev. Immunol 14, 109–121 (2014). [PubMed: 24457485]
23. Brähler S, Zinselmeyer BH, Raju S, Nitschke M, Suleiman H, Saunders BT, Johnson MW, Böhner AMC, Viehmann SF, Theisen DJ, Kretzer NM, Briseño CG, Zaitsev K, Ornatsky O, Chang Q, Carrero JA, Kopp JB, Artyomov MN, Kurts C, Murphy KM, Miner JH, Shaw AS, Opposing Roles of Dendritic Cell Subsets in Experimental GN, J. Am. Soc. Nephrol 29, 138–154 (2018). [PubMed: 29217759]
24. Durai V, Bagadia P, Granja JM, Satpathy AT, Kulkarni DH, Davidson JT, Wu R, Patel SJ, Iwata A, Liu T-T, Huang X, Briseño CG, Grajales-Reyes GE, Wöhner M, Tagoh H, Kee BL, Newberry RD, Busslinger M, Chang HY, Murphy TL, Murphy KM, Cryptic activation of an Irf8 enhancer governs cDC1 fate specification, Nat. Immunol 20, 1161–1173 (2019). [PubMed: 31406378]
25. Mempel TR, Henrickson SE, von Andrian UH, T-cell priming by dendritic cells in lymph nodes occurs in three distinct phases, Nature 427, 154–159 (2004). [PubMed: 14712275]
26. Hwang LN, Yu Z, Palmer DC, Restifo NP, The In vivo Expansion Rate of Properly Stimulated Transferred CD8+ T Cells Exceeds That of an Aggressively Growing Mouse Tumor, Cancer Res. 66, 1132–1138 (2006). [PubMed: 16424050]
27. Chu HH, Chan S-W, Gosling JP, Blanchard N, Tsitsiklis A, Lythe G, Shastri N, Molina-París C, Robey EA, Continuous Effector CD8+ T Cell Production in a Controlled Persistent Infection Is Sustained by a Proliferative Intermediate Population, Immunity 45, 159–171 (2016). [PubMed: 27421704]
28. Cantor J, Slepak M, Ege N, Chang JT, Ginsberg MH, Loss of T Cell CD98 H Chain Specifically Ablates T Cell Clonal Expansion and Protects from Autoimmunity, J. Immunol 187, 851–860 (2011). [PubMed: 21670318]
29. D'Souza WN, Lefrançois L, IL-2 Is Not Required for the Initiation of CD8 T Cell Cycling but Sustains Expansion, J. Immunol 171, 5727–5735 (2003). [PubMed: 14634080]
30. Wang J, Kubes P, A Reservoir of Mature Cavity Macrophages that Can Rapidly Invade Visceral Organs to Affect Tissue Repair, Cell 165, 668–678 (2016). [PubMed: 27062926]
31. Frickel E-M, Hunter CA, Lessons from Toxoplasma: Host responses that mediate parasite control and the microbial effectors that subvert them, J. Exp. Med 218, e20201314 (2021). [PubMed: 34670268]
32. Hickman HD, Takeda K, Skon CN, Murray FR, Hensley SE, Loomis J, Barber GN, Bennink JR, Yewdell JW, Direct priming of antiviral CD8+ T cells in the peripheral interfollicular region of lymph nodes, Nat. Immunol 9, 155–165 (2008). [PubMed: 18193049]

33. Dudziak D, Kamphorst AO, Heidkamp GF, Buchholz VR, Trumpfheller C, Yamazaki S, Cheong C, Liu K, Lee H-W, Park CG, Steinman RM, Nussenzweig MC, Differential Antigen Processing by Dendritic Cell Subsets in Vivo, Science 315, 107–111 (2007). [PubMed: 17204652]

34. Mohapatra AD, Tirrell I, Bénéchet AP, Pattnayak S, Khanna KM, Srivastava PK, Cross-dressing of CD8α+ Dendritic Cells with Antigens from Live Mouse Tumor Cells Is a Major Mechanism of Cross-priming, Cancer Immunol. Res 8, 1287–1299 (2020). [PubMed: 32759362]

35. Duong E, Fessenden TB, Lutz E, Dinter T, Yim L, Blatt S, Bhutkar A, Wittrup KD, Spranger S, Type I interferon activates MHC class I-dressed CD11b+ conventional dendritic cells to promote protective anti-tumor CD8+ T cell immunity, Immunity 55, 308–323.e9 (2022). [PubMed: 34800368]

36. Gérard A, Khan O, Beemiller P, Oswald E, Hu J, Matloubian M, Krummel MF, Secondary T cell–T cell synaptic interactions drive the differentiation of protective CD8+ T cells, Nat. Immunol 14, 356–363 (2013). [PubMed: 23475183]

37. Marchingo JM, Kan A, Sutherland RM, Duffy KR, Wellard CJ, Belz GT, Lew AM, Dowling MR, Heinzel S, Hodgkin PD, Antigen affinity, costimulation, and cytokine inputs sum linearly to amplify T cell expansion, Science 346, 1123–1127 (2014). [PubMed: 25430770]

38. Linderman JJ, Riggs T, Pande M, Miller M, Marino S, Kirschner DE, Characterizing the Dynamics of CD4+ T Cell Priming within a Lymph Node, J. Immunol 184, 2873–2885 (2010). [PubMed: 20154206]

39. Handel A, Gruta NLL, Thomas PG, Simulation modelling for immunologists, Nat. Rev. Immunol 20, 186–195 (2020). [PubMed: 31804613]

40. Adams TA, Seider WD, Practical optimization of complex chemical processes with tight constraints, Comput. Chem. Eng 32, 2099–2112 (2008).

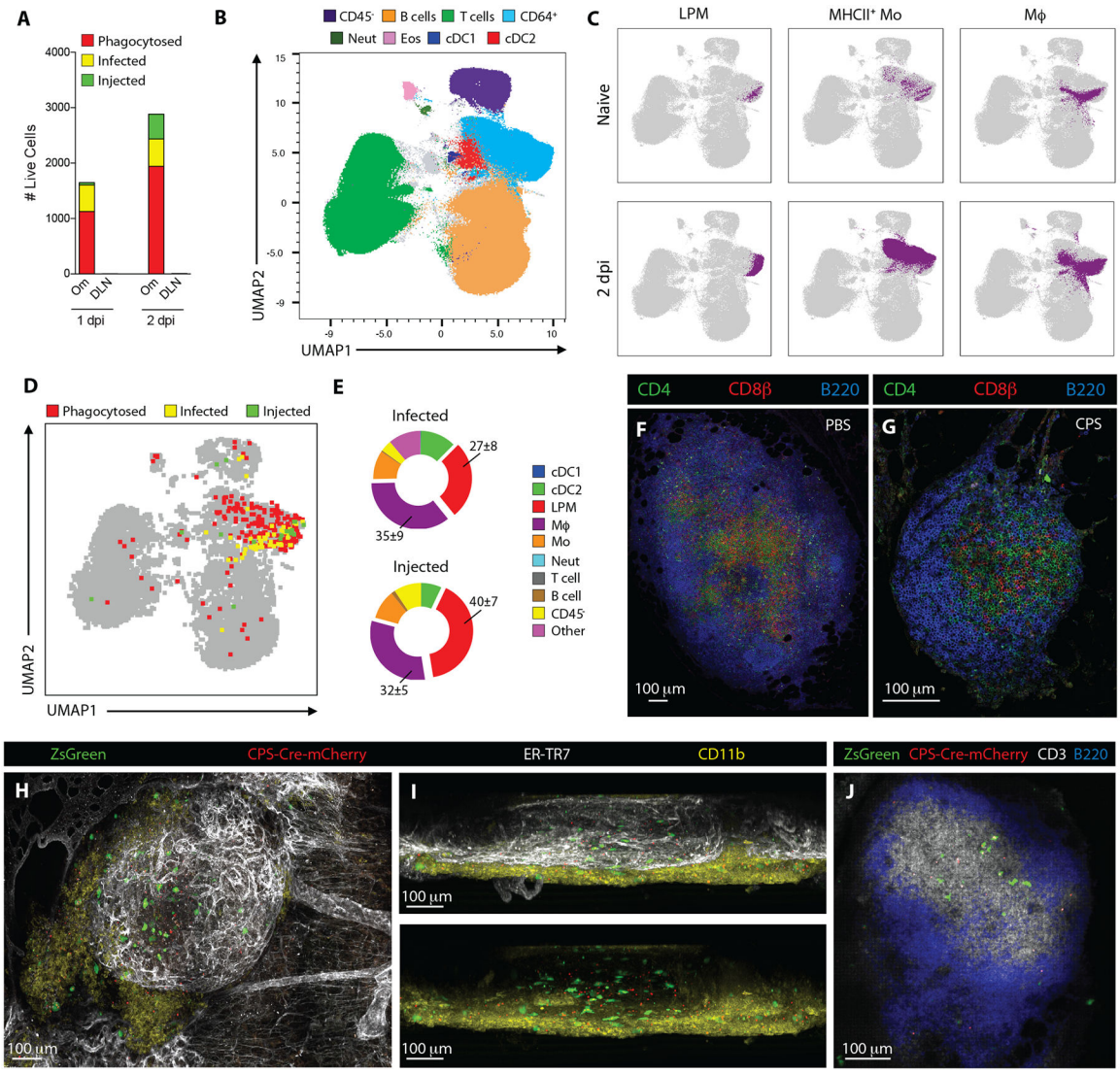


**Fig. 1. CPS immunization results in antigen transport to MS**

(**A**) Intraperitoneal immunization of Ai6 mice with CPS-Cre-mCherry parasites. Quantification of cells phagocytosing the parasite (Toxo$^+$ZsGreen$^-$), infected cells (Toxo$^+$ZsGreen$^+$), and injected cells (Toxo$^-$ZsGreen$^+$) from the peritoneum to the omentum and DLN at 1 and 2 dpi. Data represent summation of the means.

(**B** to **E**) UMAP projection of cellularity of the omentum of naïve and CPS-Cre-mCherry-immunized Ai6 mice at 2 dpi. (B) Color-coded for clusters of non-hematopoietic cells (CD45$^-$), B cells (CD45$^+$CD64$^-$FcER1α$^-$cKit$^-$SiglecH$^-$Ly6G$^-$CD19$^+$MHCII$^+$B220$^+$), T cells (CD45$^+$CD64$^-$FcER1α$^-$cKit$^-$SiglecH$^-$Ly6G$^-$TCRβ$^+$CD5$^+$MHCII$^-$CD3$^+$), CD64$^+$ (CD45$^+$CD64$^+$CD11b$^+$), Neutrophils (CD45$^+$CD64$^-$FcER1α$^-$cKit$^-$SiglecH$^-$Ly6G$^+$), Eosinophils (CD45$^+$CD64$^-$FcER1α$^-$cKit$^-$SiglecH$^-$Ly6G$^-$TCRβ$^-$CD5$^-$CD19$^-$NK1.1$^-$CD3$^-$CD11b$^+$SiglecF$^+$), cDC1 (CD45$^+$CD64$^-$FcER1α$^-$cKit$^-$SiglecH$^-$CD11c$^+$MHCII$^+$XCR1$^+$CD11b$^-$), cDC2 (CD45$^+$CD64$^-$FcER1α$^-$cKit$^-$SiglecH$^-$CD11c$^+$MHCII$^+$XCR1$^-$CD11b$^+$).

(C) UMAP projection of changes in the $CD64^+$ population between naïve (top) and immunized (bottom) Ai6 mice. Color-coded for indicated cell-type, LPM ($CD45^+CD64^+CD11b^+CD102^+$), $MHCII^+$ Mo ($CD45^+CD64^+CD11b^+CD102^-MHCII^+Ly6C^+$), Mϕ ($CD45^+CD64^+CD11b^+CD102^+MHCII^+Ly6C^-$).
(D) Cells phagocytosing parasites (red), infected cells (yellow), and injected cells (green) in the omentum color-coded on UMAP projection from (B).
(E) Quantification of cellular distribution of infected and injected cells from immunized omenta. DLN, Draining LN; UMAP, Uniform Manifold Approximation and Projection; Neut, Neutrophil; Eos, eosinophils; cDC, conventional dendritic cell; LPM, large peritoneal macrophage; Mo, monocyte; Mϕ, macrophage.
(**F** and **G**) Omentum MS from WT mice injected with PBS or $10^5$ CPS parasites at 2 dpi showing regions enriched in B cells and T cells. CD4 (green), CD8β (red), B220 (blue).
(**H** to **J**) MS from Ai6 mice immunized with $10^5$ CPS-Cre-mCherry parasites at 2 dpi. (H and I) ZsGreen (green), CPS-Cre-mCherry (red), ER-TR7 (white), CD11b (yellow). (J) ZsGreen (green), CPS-Cre-mCherry (red), CD3 (white), B220 (blue). Data are representative plots from 2–3 experiments using 4–5 mice.

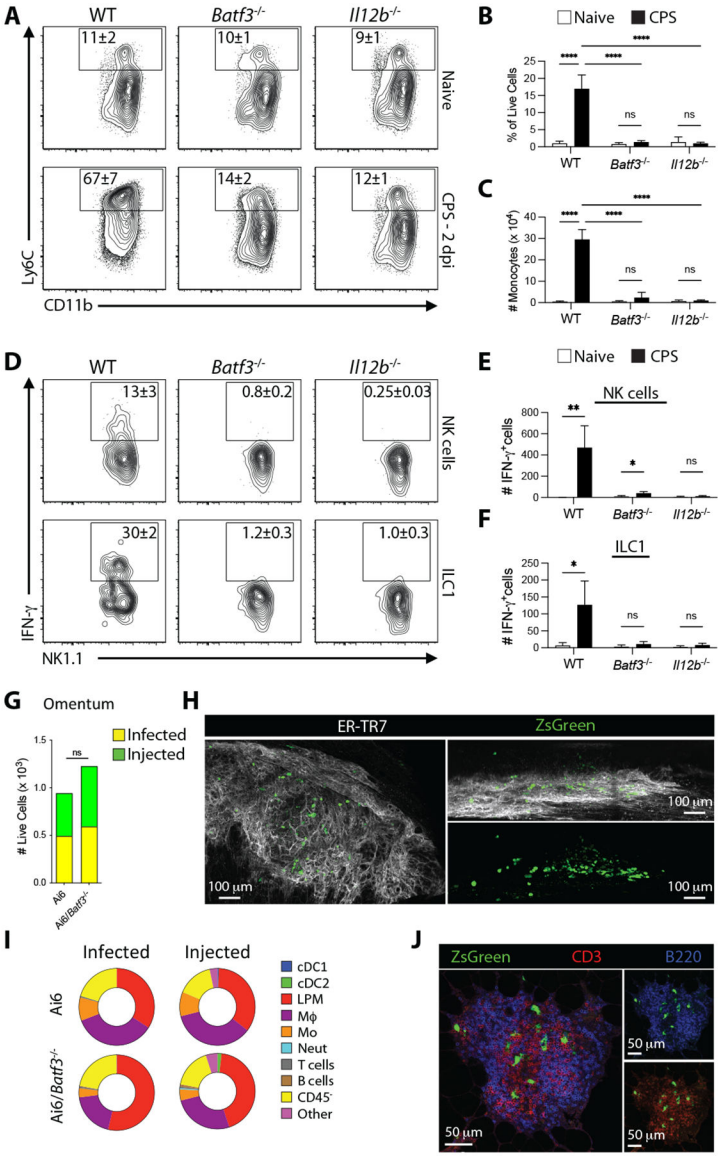


**Fig. 2. Recruitment of innate immune cells to MS requires cDC1 and IL-12**

(**A** to **C**) Quantification of monocytes in the omenta of WT, *Batf3*$^{-/-}$ and *Il12b*$^{-/-}$ mice after immunization with CPS parasites (2 dpi). (A) Flow cytometry analysis of monocytes (CD64$^{+}$CD11b$^{+}$CD102$^{-}$Ly6C$^{HI}$).

(B and C) Quantification of monocytes (B) as a fraction of live cells in the omentum and (C) the number of monocytes in the omentum. Data represent 1 experiment from 2–3 independent experiments with 4–5 mice.

(**D** to **F**) Quantification of IFN-γ production by ILCs in the omenta of WT, *Batf3*$^{-/-}$, and *Il12b*$^{-/-}$ mice after immunization with CPS parasites (1 dpi). (D) Flow cytometry analysis of NK cells (Lin$^{-}$NK1.1$^{+}$NKp46$^{+}$EOMES$^{+}$CD200R$^{-}$) and ILC1s (Lin$^{-}$NK1.1$^{+}$NKp46$^{+}$EOMES$^{-}$CD200R$^{+}$) producing IFN-γ.

(E and F) Quantification of total number of (E) NK cells and (F) ILC1s producing IFN-γ. Lin (CD3, CD5, CD19, B220, F4/80).

(**G**) Quantification of numbers of infected and injected Live Cells in the omentum of Ai6 and Ai6/*Batf3*$^{-/-}$ mice after immunization with CPS-Cre-mCherry parasites (2 dpi).
(**H**) 3D rendering of infected cells in MS of Ai6/*Batf3*$^{-/-}$ mice immunized with CPS-Cre-mCherry parasites (2 dpi). ER-TR7 (gray), ZsGreen (green).
(**I**) Cellular distribution of infected and injected cells in the omenta of Ai6 and Ai6/*Batf3*$^{-/-}$ mice with same gating strategy as (Fig. 1B).
(**J**) Z slice showing infected cells in T cell enriched region of MS of Ai6/*Batf3*$^{-/-}$ mice immunized with CPS-Cre-mCherry parasites (2 dpi). ZsGreen (green), CD3 (red), B220 (blue).
Data are representative plots from 2–3 independent experiments all using 4–5 mice. (B, C, E, and F) Bar graphs indicate mean ± SD. (G) Bar graph indicates summation of means. Data analyzed by (B and C) 2-way ANOVA or (E, F, and G) unpaired T test. ns, not significant; *p < 0.05; **p < 0.01; ****p < 0.0001.

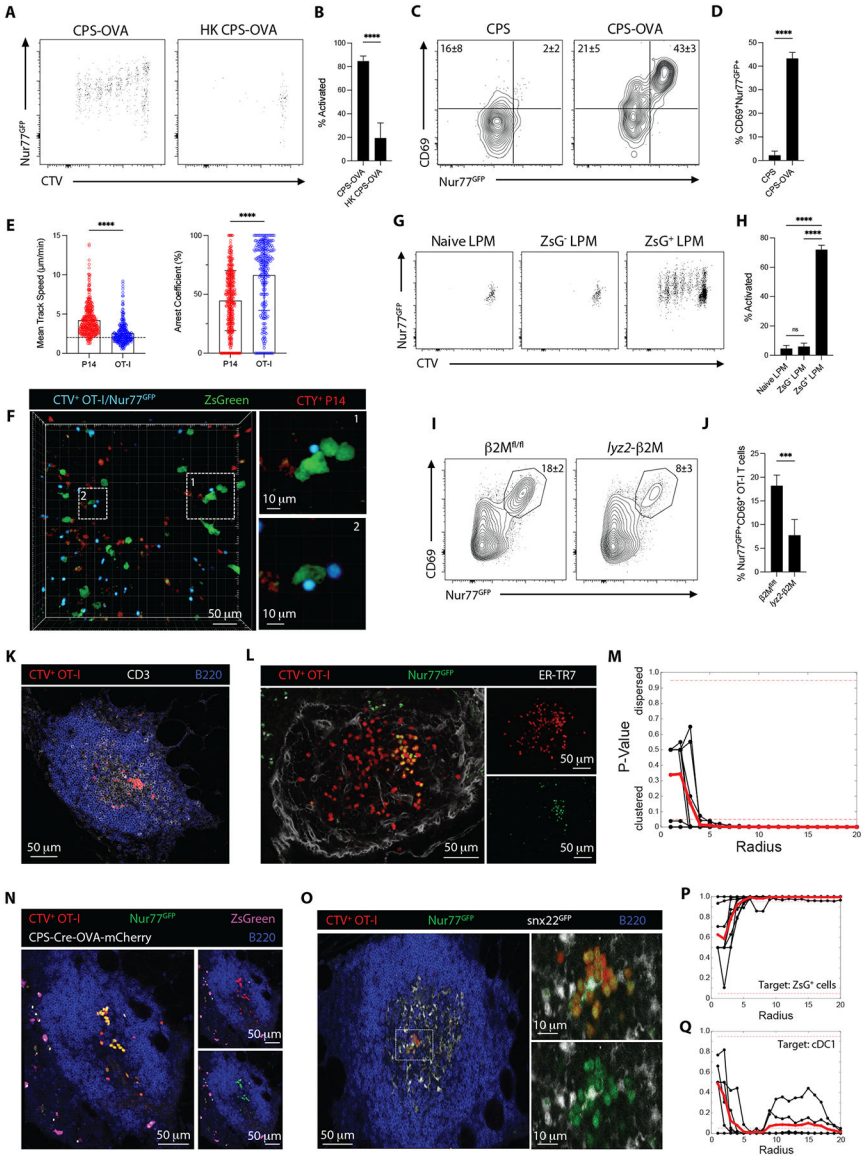


**Fig. 3. CD8$^+$ T cell activation in the omentum**

(**A** and **B**) Intravenous transfer of $10^6$ CTV-labeled OT-I/Nur77$^{GFP}$ T cells into WT mice that were immunized i.p. with either CPS-OVA or heat-killed (HK) CPS-OVA parasites 24 hr later. (A) Flow cytometric analysis of transferred CTV$^+$ OT-I/Nur77$^{GFP}$ T cells in the omentum of recipient WT mice at 3 dpi.

(B) Quantification of the activated (Nur77$^{GFP+}$ and divided) OT-I/Nur77$^{GFP}$ T cells.

(**C** and **D**) Intraperitoneal transfer of $10^6$ CTV-labeled OT-I/Nur77$^{GFP}$ T cells into WT mice that were immunized with CPS or CPS-OVA parasites 2 hr later. (C) Flow cytometric analysis of transferred CTV$^+$ OT-I/Nur77$^{GFP}$ T cells in the omentum of recipient WT mice at 18 hpi measured.

(D) Quantification of the fraction of activated (CD69$^+$Nur77$^{GFP+}$) OT-I/Nur77$^{GFP}$ T cells in the omentum.

(**E** and **F**) Intravital imaging of OT-I/Nur77$^{GFP}$ T cells and P14 T cells in the MS of Ai6 mice immunized with CPS-Cre-OVA-mCherry at 20 hpi. At 18 hpi, 2 × $10^5$ CTV-labeled OT-I/Nur77$^{GFP}$ and 2 × $10^5$ CTY-labeled P14 T cells were transferred i.p. into Ai6 mice, and 2 hours later the omentum was imaged. (E) Analysis of the Mean Track Speed and Arrest Coefficient for OT-I/Nur77$^{GFP}$ and P14 T cells.

(F) The association of CTV-labeled OT-I/Nur77$^{GFP}$ and CTY-labeled P14 with infected ZsGreen$^{+}$ cells in the MS. CTV (cyan), ZsGreen (green), CTY (red).

(**G** and **H**) Naïve OT-I/Nur77$^{GFP}$ T cell priming *in vitro* for 72 hr by naïve, uninfected (ZsG$^{-}$), or infected (ZsG$^{+}$) LPM sorted from naive or immunized (5 × $10^5$ CPS-Cre-OVA-mCherry parasites i.p. for 18 h) Ai6 mice. (G) Flow cytometric analysis of CTV$^{+}$ OT-I/Nur77$^{GFP}$ T cells by each group of LPM.

(H) Quantification of the fraction of activated (Nur77$^{GFP+}$, divided) OT-I/Nur77$^{GFP}$ T cells in each group.

(**I** and **J**) Intraperitoneal transfer of $10^6$ OT-I/Nur77$^{GFP}$ T cells into β2M$^{fl/fl}$ or *Lyz2*-β2M mice that were immunized with CPS-OVA parasites 2 hr later. (I) Flow cytometric analysis of transferred OT-I/Nur77$^{GFP}$ T cells in the omentum of recipient mice at 18 hpi.

(J) Quantification of the fraction of activated (CD69$^{+}$Nur77$^{GFP+}$) OT-I/Nur77$^{GFP}$ T cells in the omentum.

(**K** to **M**) Imaging and analysis of 5 × $10^5$ i.p.-transferred CTV-labeled OT-I/Nur77$^{GFP}$ T cell clustering in the MS of WT mice immunized with CPS-OVA at 18 hpi. (K) OT-I T cell clustering in the T cell enriched area of the MS. CTV (red), CD3 (gray), B220 (blue).

(L) CTV$^{+}$ OT-I/Nur77$^{GFP+}$ T cell clustering in MS. CTV (red), Nur77$^{GFP}$ (green), ER-TR7 (white).

(M) K-function statistical analysis of Nur77$^{GFP+}$ OT-I T cell clustering in 9 individual MS (black lines) from 2 individual mice was averaged (red line). Dashed red lines indicate significant P values of 0.05 and 0.95.

(**N** to **Q**) Imaging and analysis of 5 × $10^5$ i.p.-transferred CTV-labeled OT-I/Nur77$^{GFP}$ T cells clustering in the MS of Ai6 or *Snx22*$^{GFP/+}$ mice that were immunized with CPS-Cre-OVA-mCherry parasites at 18 hpi. (N) Imaging of infected cells and CTV$^{+}$ OT-I/Nur77$^{GFP+}$ T cell clustering in MS of Ai6 mice. CTV (red), Nur77$^{GFP}$ (green), ZsGreen (magenta), CPS-Cre-OVA-mCherry (white), B220 (blue). Nur77$^{GFP}$ and ZsGreen were distinguished and pseudocolored using Imaris imaging software.

(O) Immunofluorescence imaging of cDC1 and CTV$^{+}$ OT-I/Nur77$^{GFP+}$ T cell clustering in the MS of *Snx22*$^{GFP/+}$ mice. CTV (red), Nur77$^{GFP}$ (green), *Snx22*$^{GFP}$ (gray), B220 (blue). Nur77$^{GFP}$ and *Snx22*$^{GFP}$ were distinguished and pseudocolored using Imaris imaging software.

(P and Q) Cross K-function statistical analysis of Nur77$^{GFP+}$ OT-I T cell clusters compared to the ZsGreen$^{+}$ cells in Ai6 mice (P) or cDC1 in *Snx22*$^{GFP/+}$ mice (Q). Analysis of clustering in (P) 9 individual MS (black lines) from 2 individual mice or (Q) 6 individual MS (black lines) from 2 individual mice. Average values indicated by solid red lines, dashed red lines indicate significant P values of 0.05 and 0.95.

CTV, CellTrace Violet; CTY, CellTrace Yellow. Data are representative plots from (B and H) 2, (D, J, P, and Q) 3, or (M) 7 independent experiments all using 2–6 mice. (B, D, E, H, and J) Bar graphs indicate mean±SD. Data analyzed by (H) One-way ANOVA or (B, D, E, and G) unpaired T test. ns, not significant; ***p < 0.001; ****p < 0.0001.

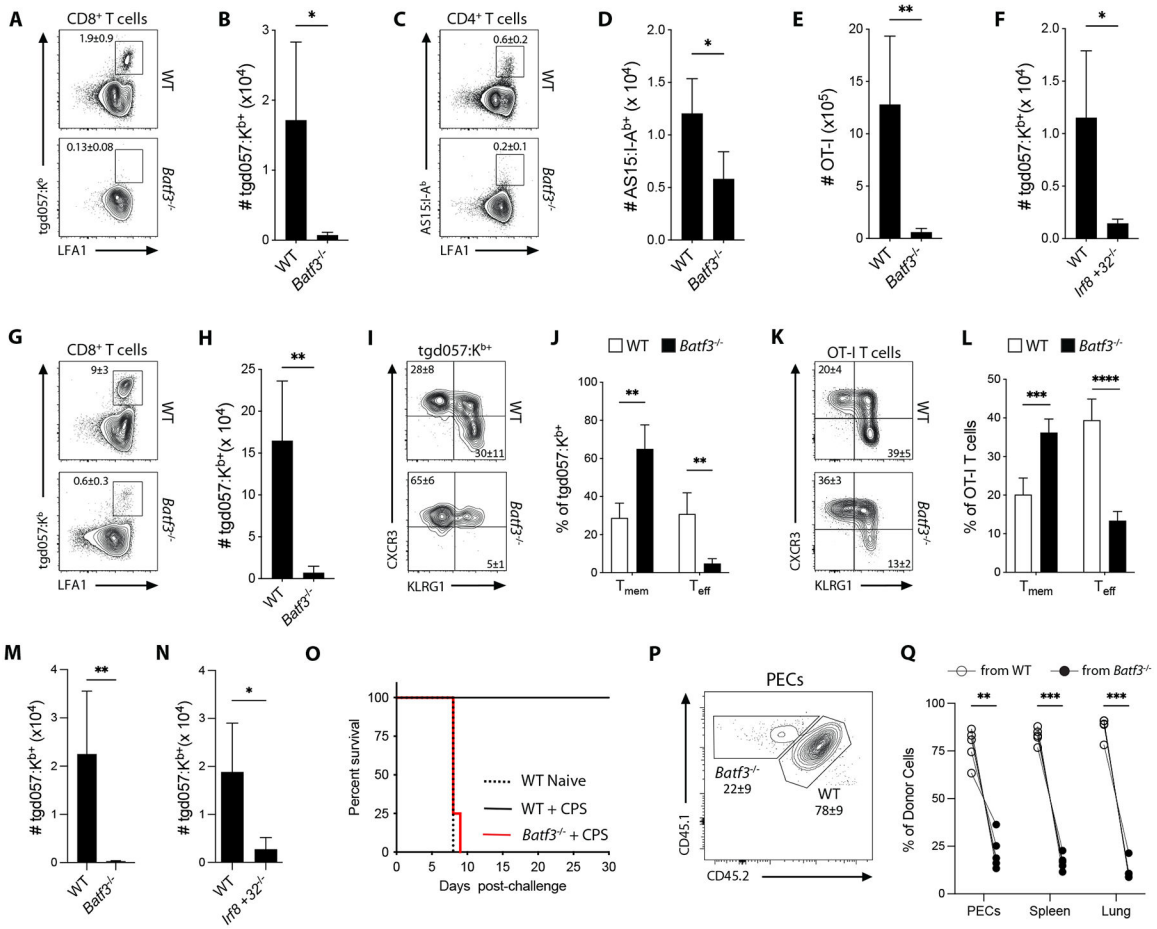


**Fig. 4. T cell responses to CPS require cDC1**

(**A** to **D**) WT and *Batf3*$^{-/-}$ mice were immunized with CPS parasites. T cell responses in the spleen were assessed at 9 dpi. (A) Flow cytometric analysis of *T. gondii*-specific (tgd057:K$^{b+}$) CD8$^{+}$ T cells.

(B) Quantification of tgd057:K$^{b+}$ CD8$^{+}$ T cells.

(C) Flow cytometric analysis of *T. gondii*-specific (AS15:I-A$^{b+}$) CD4$^{+}$ T cells.

(D) Quantification of AS15:I-A$^{b+}$ CD4$^{+}$ T cells.

(**E**) Intravenous transfer of 5 × 10$^{3}$ congenically distinct OT-I T cells into WT and *Batf3*$^{-/-}$ mice that were immunized with CPS-OVA parasites 24 hr later. Quantification of OT-I T cells in the spleen at 8 dpi

(**F**) Quantification of the number of tgd057:K$^{b+}$ CD8$^{+}$ T cells in the spleens of WT and *Irf8 +32*$^{-/-}$ mice immunized i.p. with CPS parasites at 11 dpi.

(**G** to **J**) WT and *Batf3*$^{-/-}$ mice were immunized i.p. with CPS parasites. T cell responses in the peritoneum were assessed at 9 dpi. (G) Flow cytometric analysis of tgd057:K$^{b+}$ CD8$^{+}$ T cells.

(H) Quantification of tgd057:K$^{b+}$ CD8$^{+}$ T cells.

(I) Flow cytometric analysis of the T$_{mem}$ (CXCR3$^{+}$KLRG1$^{-}$) and T$_{eff}$ (CXCR3$^{-}$KLRG1$^{+}$) phenotypes of tgd057:K$^{b+}$ CD8$^{+}$ T cells.

(J) Quantification of the fraction of T$_{mem}$ and T$_{eff}$ phenotypes.

(**K** and **L**) Intravenous transfer of $5 \times 10^3$ congenically distinct OT-I T cells into WT and *Batf3*$^{-/-}$ mice that were immunized i.p. with CPS-OVA parasites 24 hr later. T cell responses in the peritoneum were assessed at 8 dpi. (K) Flow cytometric analysis of the $T_{mem}$ and $T_{eff}$ phenotypes of OT-I T cells.

(L) Quantification of the fraction of the $T_{mem}$ and $T_{eff}$ phenotypes of OT-I T cells.

(**M** and **N**) WT and *Batf3*$^{-/-}$ (M) or *Irf8* +*32*$^{-/-}$ (N) mice were immunized with $10^5$ CPS parasites. Quantification of the number of tgd057:$K^{b+}$ $CD8^+$ T cells in the spleen at 30 dpi.

(**O**) WT and *Batf3*$^{-/-}$ mice were immunized with CPS parasites. At 30 dpi, immunized WT and *Batf3*$^{-/-}$ mice and naïve WT mice were challenged with the lethal RH strain of *T. gondii* and survival assessed.

(**P** and **Q**) (P) Flow cytometric analysis of donor OT-I T cell populations sorted from CPS-OVA immunized WT ($CD45.1.2^+$) and *Batf3*$^{-/-}$ ($CD45.1^+$) mice in the peritoneum of WT recipients infected with Pru-OVA i.p. at 12 dpi.

(Q) Quantification of the fraction of donor OT-I T cells from WT and *Batf3*$^{-/-}$ mice in the peritoneum, spleen, and lungs of individual infected WT recipients.

Data are representative plots from (E, F, L, M, N, O, and Q) 2 or (B, D, H, and J) 3 independent experiments all using 4–5 mice. (B, D, E, F, H, J, L, M, and N) Bar graphs indicate mean±SD. (Q) Plots of paired donor cell fractions for each mouse. Data analyzed by (B, D, E, F, H, J, L, M, and N) unpaired T test or (Q) paired T test. *$p < 0.05$; **$p < 0.01$, ***$p < 0.0001$.

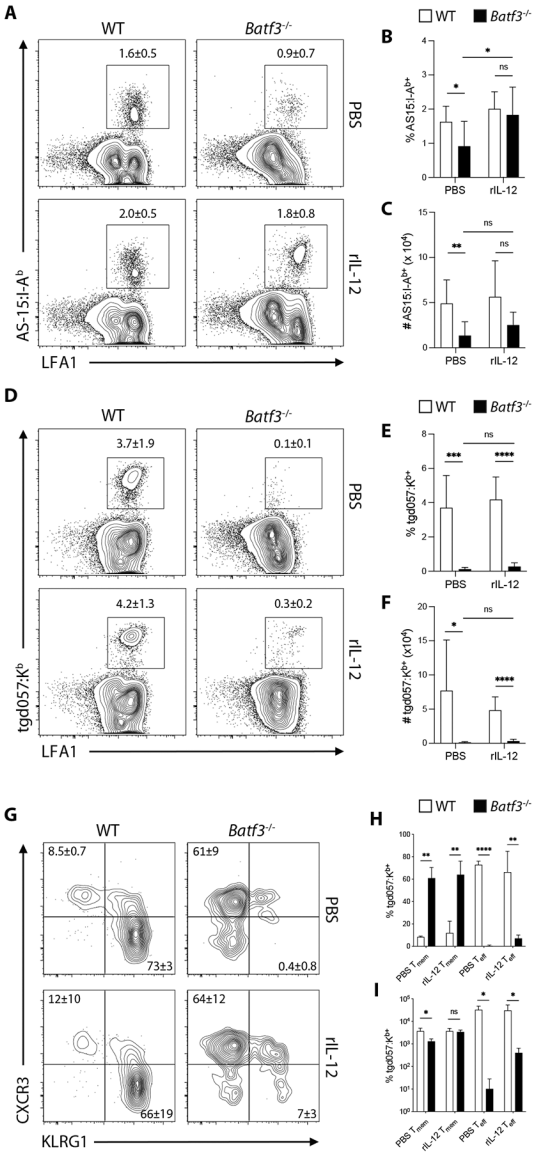


**Fig. 5. IL-12-independent role for cDC1s in the CD8$^+$ T cell response to CPS**

(**A** to **I**) WT and *Batf3*$^{-/-}$ mice were immunized with CPS parasites followed by i.p. administration of either PBS or 200 ng rIL-12 at 0, 24, and 48 hpi. T cell responses in the peritoneum were assessed via flow cytometry at 11 dpi. (A) Representative plots of AS15:I-A$^{b+}$ CD4$^+$ T cells.

(B and C) The fraction and number of AS15:I-A$^{b+}$ CD4$^+$ T cells.

(D) Representative plots of tgd057:K$^{b+}$ CD8$^+$ T cells.

(E and F) The fraction and number of tgd057:K$^{b+}$ CD8$^+$ T cells. Data (n = 6–8) represent data from 2 independent experiments.

(G) Representative plots of the $T_{eff}$ and $T_{mem}$ phenotypes of tgd057:K$^{b+}$ CD8$^+$ T cells.

(H and I) The fraction and number of $T_{mem}$ or $T_{eff}$ phenotypes of tgd057:K$^{b+}$ CD8$^+$ T cells. Data in (B, C, E, and F) are pooled from 2 independent experiments with 3–5 mice, and (H and I) are representative of 2 independent experiments with 3–5 mice. Bar graphs indicate

mean±SD. All statistical comparisons were unpaired T test. ns, not significant; *p < 0.05; **p < 0.01; ***p < 0.001; ****p < 0.0001.

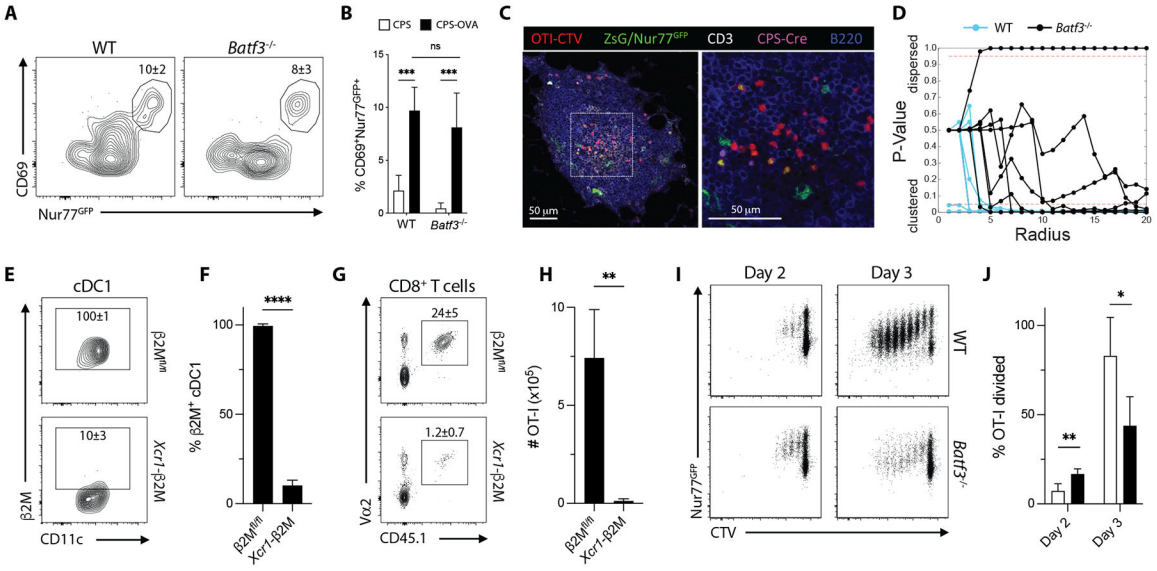


**Fig. 6. cDC1 are not required for CD8$^+$ T cell activation**

(**A** and **B**) Intraperitoneal transfer of $10^6$ congenically distinct OT-I/Nur77$^{GFP}$ T cells into WT and *Batf3*$^{-/-}$ mice that were immunized with CPS or CPS-OVA parasites 2 hr later. (A) Flow cytometric analysis of OT-I/Nur77$^{GFP}$ T cells.

(B) Quantification of the fraction of activated (CD69$^+$Nur77$^{GFP+}$) OT-I/Nur77$^{GFP}$ T cells in the omentum.

(**C** and **D**) Imaging of $5 \times 10^5$ i.p. transferred CTV-labeled OT-I/Nur77$^{GFP}$ T cells clusters in the MS of Ai6/*Batf3*$^{-/-}$ mice that were immunized with CPS-Cre-OVA-mCherry parasites at 18 hpi. (C) Images of CTV$^+$ OT-I/Nur77$^{GFP}$ T cell clustering. CTV (red), ZsGreen, Nur77$^{GFP}$ (green), CD3 (gray), CPS-Cre-OVA-mCherry (magenta), B220 (blue).

(D) K-function statistical analysis of Nur77$^{GFP+}$ OT-I T cell clustering in MS from WT mice (cyan lines, taken from Fig. 3M) and *Batf3*$^{-/-}$ mice (black lines). Analysis in *Batf3*$^{-/-}$ mice was done for 7 individual MS from 2 individual mice.

(**E** to **H**) Intravenous transfer of $5 \times 10^3$ OT-I/Nur77$^{GFP}$ T cells into β2M$^{fl/fl}$ and *Xcr1*-β2M mice immunized with CPS-OVA parasites 24 hr later. (E) Flow cytometric analysis of the efficiency of β2M deletion in cDC1 in the spleen of β2M$^{fl/fl}$ and *Xcr1*-β2M mice at 7 dpi.

(F) Quantification of the fraction of β2M$^+$ cDC1 in the spleen at 7 dpi.

(G) Flow cytometric analysis of the OT-I T cell population in β2M$^{fl/fl}$ and *Xcr1*-β2M mice in the spleen at 7 dpi.

(H) Quantification of OT-I T cells in the spleen at 7 dpi.

(**I** and **J**) Intraperitoneal transfer of $5 \times 10^5$ CTV-labeled OT-I/Nur77$^{GFP}$ T cells into WT and *Batf3*$^{-/-}$ mice immunized with CPS-OVA parasites 2 hr later. (I) Flow cytometric analysis of the activation (Nur77$^{GFP+}$) and division (CTV dilution) of OT-I T cells in the omentum at 2 and 3 dpi.

(J) Quantification of the fraction of OT-I T cells that have undergone division.

Data are representative plots from (B, F, H, and J) 2 or (D) 4 independent experiments all using 3–6 mice. Bar graphs indicate mean±SD. Data analyzed by unpaired T test. ns = not significant, *p < 0.05; **p < 0.01, ***p < 0.001, ****p < 0.0001.

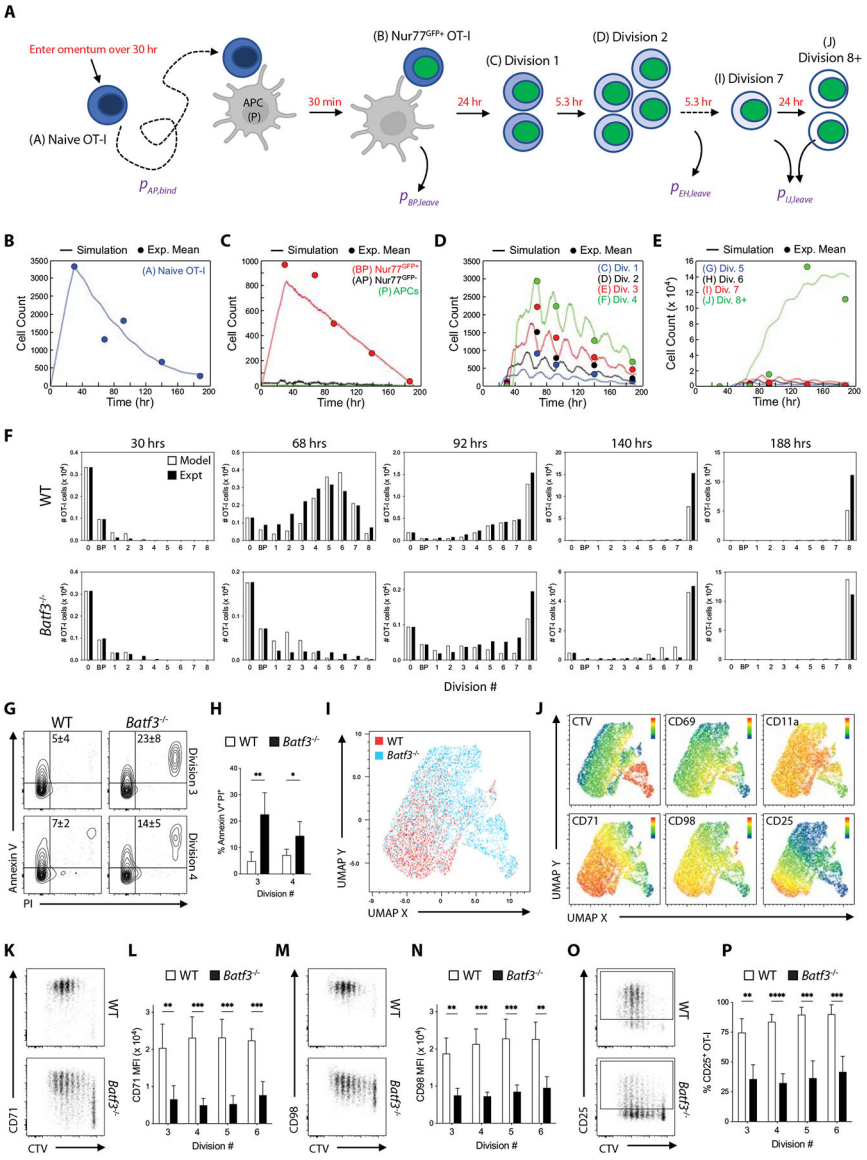


**Fig. 7. Stochastic modeling implicates defect in OT-I expansion in *Batf3*$^{-/-}$ mice**

(**A**) Schematic of STORE model of OT-I T cell activation depicting the set (red text) and variable (purple text) variables.

(**B** to **P**) Intraperitoneal transfer of 5 × $10^5$ OT-I/Nur77$^{GFP}$ T cells into WT and *Batf3*$^{-/-}$ mice immunized with CPS-OVA parasites 2 hr later.

(B-E) Representative plots from a simulation of the STORE model where solid lines indicate simulation data and filled circles indicate number of OT-I T cells in each group measured by flow cytometry.

(B) The number of naïve OT-I T cells over time.

(C) The numbers of unbound APCs and APC binding pairs with Nur77$^{GFP-}$ (AP) and Nur77$^{GFP+}$ (BP) OT-I T cells over time.

(D) The number OT-I T cells in divisions 1–4 versus time.

(E) The number of OT-I T cells in divisions 5–8+ versus time.

(F) The number of OT-I T cells at different time points from simulations and experimental data (average) in WT and *Batf3*$^{-/-}$ recipient mice.
(G) Flow cytometric analysis of OT-I T cell death (Annexin V$^{+}$ PI$^{+}$) in divisions 3 and 4 in WT and *Batf3*$^{-/-}$ mice.
(H) The fraction of dead OT-I T cells in divisions 3 and 4 in WT and *Batf3*$^{-/-}$ mice.
(I) UMAP projection of OT-I T cells from WT and *Batf3*$^{-/-}$ mice.
(J) Heat map overlay of CTV and expression levels of CD69, CD11a, CD71, CD98, and CD25 by OT-I T cells from WT and *Batf3*$^{-/-}$ mice on UMAP projection from (I).
(K-L) Flow cytometric analysis of the expression of CD71, and MFI of CD71 expression by divisions 3–6 of OT-I T cells from WT and *Batf3*$^{-/-}$ mice.
(M-N) Flow cytometric analysis of the expression of CD98, and MFI by divisions 3–6 of OT-I T cells from WT and *Batf3*$^{-/-}$ mice.
(O-P) Flow cytometric analysis of the expression of CD25, and quantification of the fraction of CD25$^{+}$ OT-I T cells in divisions 3–6 from WT and *Batf3*$^{-/-}$ mice.
STORE, STochastic Omentum REsponse; PI, propidium iodide. Data are representative plots from (F, H) 2 or (L, N, P) 6 independent experiments all using 4–5 mice. Bar graphs indicate mean±SD. Data analyzed by unpaired T test. *p < 0.05; **p < 0.01, ***p < 0.001, ****p < 0.0001.